

## Supporting Information

# Relaxation Dynamics in See-Saw Shaped Dy(III) Single-Molecule Magnets

*Katie L. M. Harriman,<sup>a</sup> Jesse Murillo,<sup>b</sup> Elizaveta A. Suturina,<sup>c</sup> Skye Fortier,<sup>\*b</sup> and Muralee*

*Murugesu<sup>\*a</sup>*

<sup>a</sup> Department of Chemistry and Biomolecular Sciences, University of Ottawa, Ottawa, Ontario K1N 6N5, Canada

<sup>b</sup> Department of Chemistry and Biochemistry, University of Texas at El Paso, El Paso, Texas 79968, USA

<sup>c</sup> Department of Chemistry, University of Bath, Claverton Down, Bath BA2 7AY, United Kingdom

\*Corresponding Authors: M. Murugesu (E-mail: m.murugesu@uottawa.ca) and S. Fortier (E-mail: asfortier@utep.edu)

Supporting Information:

**Table of Contents**

Materials and Methods .....	S5
X-ray Crystallographic Details.....	S5
Table S1. X-ray Crystallography data .....	S6
Synthesis of $[K(DME)_3][LArDy(Cl)_2]$ ( <b>1</b> ) .....	S7
Synthesis of $[K(DME)_4][LArDy(I)_2]$ ( <b>2</b> ) .....	S7
Figure S1(a). $^1H$ NMR of ( <b>1</b> ) in THF-D8 .....	S9
Figure S1(b). $^1H$ NMR of ( <b>1</b> ) in THF-D8 .....	S10
Figure S2(a). $^1H$ NMR of ( <b>2</b> ) in THF-D8 .....	S11
Figure S2(b). $^1H$ NMR of ( <b>2</b> ) in THF-D8 .....	S12
Figure S3. Room temperature electronic absorption spectra of ( <b>1</b> ) .....	S13
Figure S4. Room temperature electronic absorption spectra of ( <b>2</b> ) .....	S14
Figure S5. Intermolecular interactions in the asymmetric unit of ( <b>1</b> ) .....	S15
Figure S6. Structural metrics of the four independent molecules of ( <b>1</b> ) .....	S16
Figure S7. Structural metrics of molecule ( <b>2</b> ) .....	S17
Details of the <i>Ab Initio</i> Calculations .....	S17
Table S2. Energy splitting and <i>g</i> -tensors for Kramers doublets of ( <b>1-Dy2</b> ) .....	S18
Table S3. Parameters of the crystal field of ( <b>1-Dy2</b> ) .....	S18
Table S4. Energy splitting and <i>g</i> -tensors for Kramers doublets of ( <b>1-Dy4</b> ) .....	S19
Table S5. Parameters of the crystal field of ( <b>1-Dy4</b> ) .....	S19
Figure S8. Calculated Dipolar Energies of ( <b>1</b> ) .....	S20
Table S6. Energy splitting and <i>g</i> -tensors for Kramers doublets of ( <b>2</b> ) .....	S21
Table S7. Parameters of the crystal field of ( <b>2</b> ) .....	S21
Magnetic Measurement Details.....	S21
DC Magnetism Plots.....	S22
Figure S9. $\chi T$ vs. $T$ plots .....	S22

Figure S10. $M$ vs. $H$ and $M$ vs. $HT^{-1}$ plots of (1) .....	S23
Figure S11. $M$ vs. $H$ and $M$ vs. $HT^{-1}$ plots of (2) .....	S24
Figure S12. Zero-field-cooled and field-cooled plots .....	S25
Figure S13. $M$ vs. $H$ plot (hysteresis) of (2) .....	S26
Figure S14. $M$ vs. $H$ plots (hysteresis) of (1) and (2) .....	S27
AC Magnetism Plots.....	S28
Figure S15. $\chi'$ vs. $v$ plot of (1) @ 2-70 K and $H_{dc} = 0$ Oe .....	S28
Table S8. Fit parameters for $\chi'$ vs. $v$ plot of (1) @ 2-70 K and $H_{dc} = 0$ Oe .....	S29
Figure S16. $\chi''$ vs. $v$ plot of (1) @ 2-70 K and $H_{dc} = 0$ Oe .....	S31
Table S9. Fit parameters for $\chi''$ vs. $v$ plot of (1) @ 2-70 K and $H_{dc} = 0$ Oe .....	S32
Figure S17. Plots of fitted parameters from $\chi'$ and $\chi''$ of (1) @ 2-70 K and $H_{dc} = 0$ Oe .....	S34
Figure S18. $\chi'$ vs. $v$ plot of (2) @ 7-62 K and $H_{dc} = 0$ Oe .....	S35
Table S10. Fit parameters for $\chi'$ vs. $v$ plot of (2) @ 7-62 K and $H_{dc} = 0$ Oe .....	S36
Table S11. Fit parameters for $\chi''$ vs. $v$ plot of (2) @ 7-62 K and $H_{dc} = 0$ Oe .....	S38
Table S12. Fit parameters for $\chi''$ vs. $v$ plot of (1) @ 0-5000 Oe and 20 K .....	S40
Table S13. Fit parameters for $\chi''$ vs. $v$ plot of (2) @ 0-5000 Oe and 20 K .....	S41
Figure S19. $\tau^1$ vs. $H_{dc}$ plot of (1) and (2) .....	S42
Figure S20. $\chi'$ vs. $v$ plot of (1) @ 10-70 K and $H_{dc} = 600$ Oe .....	S43
Table S14. Fit parameters for $\chi'$ vs. $v$ plot of (1) @ 10-70 K and $H_{dc} = 600$ Oe .....	S44
Table S15. Fit parameters for $\chi''$ vs. $v$ plot of (1) @ 10-70 K and $H_{dc} = 600$ Oe .....	S46
Figure S21. Plots of fitted parameters from $\chi'$ and $\chi''$ of (1) @ 10-70 K and $H_{dc} = 600$ Oe .....	S48
Figure S22. $\chi'$ vs. $v$ plot of (2) @ 10-62 K and $H_{dc} = 1200$ Oe .....	S49
Table S16. Fit parameters for $\chi'$ vs. $v$ plot of (2) @ 10-62 K and $H_{dc} = 1200$ Oe .....	S50
Table S17. Fit parameters for $\chi''$ vs. $v$ plot of (2) @ 10-62 K and $H_{dc} = 1200$ Oe .....	S52
Figure S23. $\tau^1$ vs. $T$ plot of (1) with Eqn. 2 fit .....	S54
Figure S24. $\tau^1$ vs. $H$ plot of (2) with Eqn. 2 fit .....	S55
Table S18. Temperature dependent magnetic relaxation parameters from Eqn. 2 .....	S56

References .....	S56
------------------	-----

## Materials and Methods

All air and moisture-sensitive operations were performed in a M. Braun dry box under an atmosphere of purified dinitrogen or using high vacuum standard Schlenk techniques. Solvents were dried using a Pure Process Technology Solvent Purification System and subsequently stored under a dinitrogen atmosphere over activated 4 Å molecular sieves. Anhydrous DyCl<sub>3</sub> was purchased from Strem Chemicals Inc. at 99.9% purity. DyI<sub>3</sub>(THF)<sub>3.5</sub> was synthesized using previously reported methods.<sup>[1]</sup> [K(DME)<sub>2</sub>]<sub>2</sub>L<sup>Ar</sup> was synthesized according to the literature procedure.<sup>[2]</sup> THF-*d*<sub>8</sub> and benzene-*d*<sub>6</sub> were purchased from Cambridge Isotope Laboratories Inc. and dried over activated 4 Å molecular sieves for 24 h prior to use. Celite used for filtration was dried under vacuum while heating at 250 °C for 24 h, subsequently cooled under vacuum, and stored under dinitrogen. All NMR data reported were measured using a Bruker AVANCE III 400 MHz spectrometer, and the <sup>1</sup>H NMR spectra are referenced to SiMe<sub>4</sub> using the residual <sup>1</sup>H solvent peaks as internal standards. UV/vis-NIR spectra were recorded using a Cary 5000 spectrophotometer. Elemental analyses were performed by Midwest Microlabs, LLC. UV-vis/NIR spectra were recorded on a Cary 5000 spectrophotometer using toluene as a solvent.

## X-ray Crystallographic Details

Single crystal X-ray studies for **1** and **2** were initially carried out on a Bruker 3-axis platform diffractometer equipped with an APEX I CCD detector using a graphite monochromator with a Mo Kα X-ray source ( $\lambda = 0.71073 \text{ \AA}$ ) at 100(2) K under a flow of nitrogen gas during data collection. Alternatively, for **1**, low temperature data (15(2) K under a flow of helium gas) was collected at ChemMatCARS located at the Advanced Photon Source (APS), Argonne National Laboratory (ANL), using synchrotron radiation ( $\lambda = 0.41328 \text{ \AA}$ ) in conjunction with a Bruker D8

three-circle platform goniometer equipped with Dectris PILATUS 100 detector. Samples were coated in NVH crystallographic immersion oil and mounted on a glass fiber prior to diffraction. Data was collected using  $\phi$  and  $\omega$  scan collection strategies. Data collection and cell parameter determination were conducted using the SMART<sup>[3]</sup> program. Integration of the data and final cell parameter refinements were performed using SAINT<sup>[4]</sup> software with data absorption correction implemented through SADABS.<sup>[5]</sup> Structure solutions were completed using direct methods determinations in SHELLTL<sup>[6]</sup> or Olex2<sup>[7]</sup> crystallographic packages. All hydrogen atom positions were idealized and treated as riding on the parent atom. CCDC deposit numbers 1911732 for **1** and 1979069 for **2**.

**Table S1.** Crystallographic data for **1** and **2**.

	<b>1</b> (15K)	<b>1</b> (100K)	<b>2</b> (100K)
	[K(DME) <sub>3</sub> ][L <sup>Ar</sup> Dy(Cl) <sub>2</sub> ] (15 K)	[K(DME) <sub>3</sub> ][L <sup>Ar</sup> Dy(Cl) <sub>2</sub> ] (100 K)	[K(DME) <sub>4</sub> ][L <sup>Ar</sup> Dy(I) <sub>2</sub> ] (100 K)
empirical formula	DyN <sub>2</sub> Cl <sub>2</sub> C <sub>42</sub> H <sub>32</sub> ·K(C <sub>4</sub> H <sub>10</sub> O <sub>2</sub> ) <sub>3</sub>	DyN <sub>2</sub> Cl <sub>2</sub> C <sub>42</sub> H <sub>32</sub> ·K(C <sub>4</sub> H <sub>10</sub> O <sub>2</sub> ) <sub>3</sub>	DyN <sub>2</sub> I <sub>2</sub> C <sub>42</sub> H <sub>32</sub> ·K(C <sub>4</sub> H <sub>10</sub> O <sub>2</sub> ) <sub>4</sub>
crystal habit, color	block, red orange	block, red orange	block, red
crystal size (mm)	0.15 × 0.15 × 0.14	0.12 × 0.13 × 0.21	0.15 × 0.15 × 0.25
crystal system	monoclinic	Monoclinic	Triclinic
space group	<i>Pn</i>	<i>Cc</i>	<i>P</i> 1
volume (Å <sup>3</sup> )	11072.1(8)	11157.9(1)	3017.91(2)
<i>a</i> (Å)	21.2253(8)	21.287(2)	13.2019(4)
<i>b</i> (Å)	15.87848(7)	15.8231(9)	13.5333(4)
<i>c</i> (Å)	34.262(1)	34.353(2)	18.6052(5)
$\alpha$ (deg)	90	90	104.305(2)
$\beta$ (deg)	105.304(1)	105.354(2)	94.039(2)
$\gamma$ (deg)	90	90	108.319(2)
<i>Z</i>	2	4	1
formula weight (g/mol)	1121.76	1121.76	1881.21
density (calculated) (mg/m <sup>3</sup> )	1.342	1.338	1.035
absorption coefficient (mm <sup>-1</sup> )	1.568	0.184	1.205
<i>F</i> <sub>000</sub>	4626.3	4400	953.0
total no. reflections	267074	153297	180319
unique reflections	43121	25858	19676
final <i>R</i> indices [ <i>I</i> > 2σ( <i>I</i> )]	<i>R</i> <sub>1</sub> = 0.0464, <i>wR</i> <sub>2</sub> = 0.01259	<i>R</i> <sub>1</sub> = 0.0543, <i>wR</i> <sub>2</sub> = 0.01459	<i>R</i> <sub>1</sub> = 0.0730, <i>wR</i> <sub>2</sub> = 0.01463
largest diff. peak and hole (e <sup>-</sup> Å <sup>-3</sup> )	-2.3 and 2.2	-2.0 and 2.9	-3.43 and 4.23
GOF	1.043	1.119	1.153

**Synthesis of  $[K(DME)_3][L^{Ar}Dy(Cl)_2]$  (1).** In a 20 mL scintillation vial,  $DyCl_3$  (40.7 mg, 0.15 mmol) was added to THF (2 mL) with stirring, forming a colorless suspension. In a separate vial,  $[K(DME)_2]_2L^{Ar}$  (150.0 mg, 0.15 mmol) was dissolved in THF (4 mL), making a dark red solution. Both vials were frozen in a liquid nitrogen cooled cold-well within a glovebox. Upon thawing, the  $[K(DME)_2]_2L^{Ar}$  solution was added dropwise to the thawing, stirring  $DyCl_3$  suspension. The reaction was allowed to warm to room temperature and stirred for 12 h, resulting in a brown-yellow turbid solution. The mixture was filtered through a plug of Celite supported on a glass frit, passing a clear, brown-yellow solution. The filtrate was dried under reduced pressure to give a light brown-yellow solid. The solid was dissolved in DME (1 mL) and crystals of **1** were grown from storage of the DME solution at -25 °C for 3 days. Yield: 78.8 mg, 47.4%.  $^1H$  NMR (25 °C, 400 MHz, THF-d<sub>8</sub>):  $\delta$  -401.5 (br s), -300.3 (br s, fwhm = 8,211 Hz), -102.8 (br s), -0.2 (br s), 12.6 (br s), 33.2 and 35.8 (overlapping br s), 64.3 (br s), 117.4 (br s), 148.7 (br s), 156.9 (br s), 212.8 (br s, fwhm = 6,276 Hz), 294.9 (br s), 317.3 (br s). UV-vis (toluene, 0.29 mM, 25 °C, L·mol<sup>-1</sup>·cm<sup>-1</sup>): 297 ( $\varepsilon$  = 11,808), 406 ( $\varepsilon$  = 1,992). Anal. Calcd for  $C_{54}H_{76}N_2O_6KDyCl_2$ : C, 57.81; H, 6.84; N, 2.50. Found: C, 58.02; H, 7.00; N, 2.58.

**Synthesis of  $[K(DME)_4][L^{Ar}Dy(I)_2]$  (2).** In a 20 mL scintillation vial,  $DyI_3(\text{THF})_{3.5}$  (285.0 mg, 0.288 mmol) was added to THF (6 mL) with stirring, forming a colorless suspension. In a separate vial,  $[K(DME)_2]_2L^{Ar}$  (252.7 mg, 0.25 mmol) was dissolved in THF (4 mL), making a dark red solution. Both vials were cooled down to -35 °C in a cold-well within a glovebox. Then, the  $[K(DME)_2]_2L^{Ar}$  solution was added dropwise to the cold, stirring  $DyI_3(\text{THF})_{3.5}$  suspension. The reaction was allowed to warm to room temperature and stirred for 12 h, resulting in a brown-red turbid solution. The mixture was filtered through a plug of Celite supported on a glass frit, passing a clear, brown-red solution. The filtrate was dried under reduced pressure to give a red solid. The

solid was dissolved in DME (2 mL) and layered with pentane (2 mL). Crystals of **2** were grown from storage of the DME/pentane solution at -35 °C for 3 days. Yield: 221.7 mg, 55.7%. <sup>1</sup>H NMR (25 °C, 400 MHz, THF-d<sub>8</sub>): δ -348.6 (br s), -156.9 (br s, fwhm = 1,052 Hz), -34.9 (br s), 11.3 (br s), 11.7 (br s), 12.5 (br s), 12.7 (br s), 13.3 (br s), 45.6 (br s, fwhm = 2,764 Hz), 53.3 (br s), 73.1 (br s, fwhm = 1,488 Hz), 80.9 (br s), 93.2 (br s), 95.1(br s), 118.9 (br s), 123.4 (br s), 129.6 (br s, fwhm = 2,148 Hz), 136.9 (br s), 165.5 (br s, fwhm = 3,208 Hz), 183.9 (br s, fwhm = 1,800 Hz), 291.3 (br s), 328.2 (br s, fwhm = 3,252 Hz). UV-vis (toluene, 0.122 mM, 25 °C, L·mol<sup>-1</sup>·cm<sup>-1</sup>): 285 ( $\varepsilon$  = 18,860), 438 ( $\varepsilon$  = 1,435). Despite several independent attempts, a combustion analysis of **2** gave unsatisfactory values, which may be due to impurities or poor combustion properties.

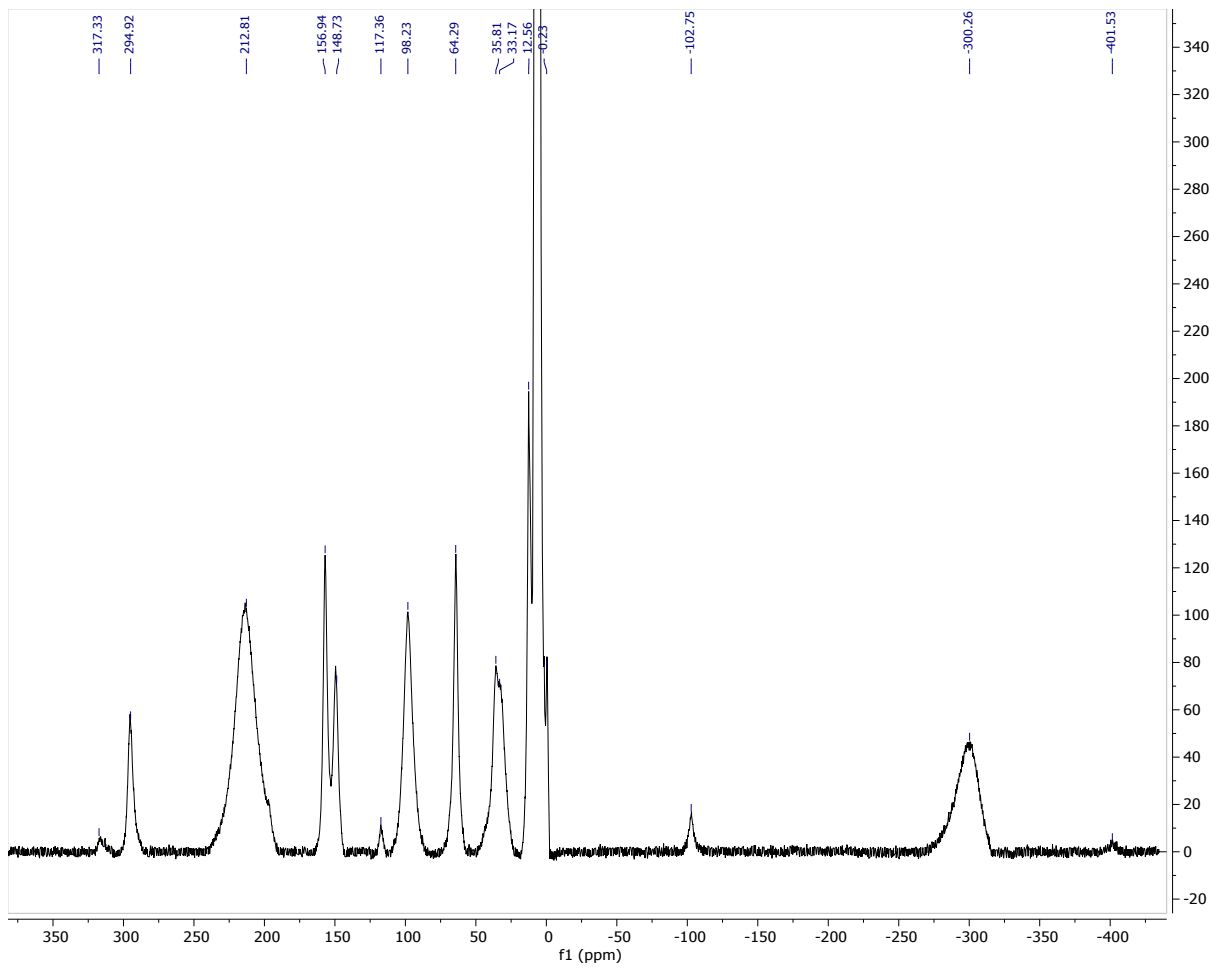


**Figure S1(a).** Baseline corrected  $^1\text{H}$  NMR (400 MHz) spectrum of **1** in  $\text{THF}-d_8$  at 25 °C.

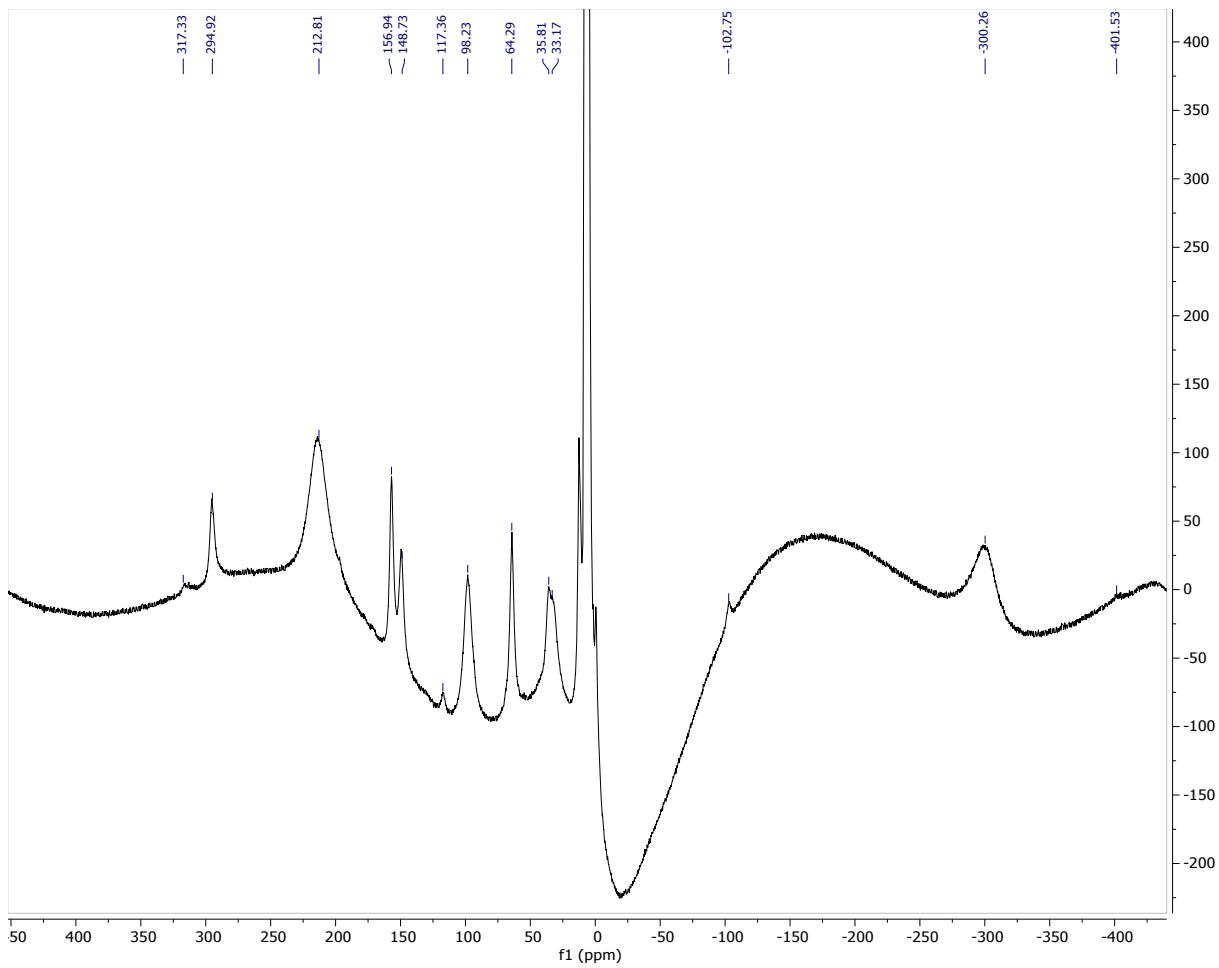


**Figure S1(b).** Baseline uncorrected  $^1\text{H}$  NMR (400 MHz) spectrum of **1** in  $\text{THF}-d_8$  at 25 °C

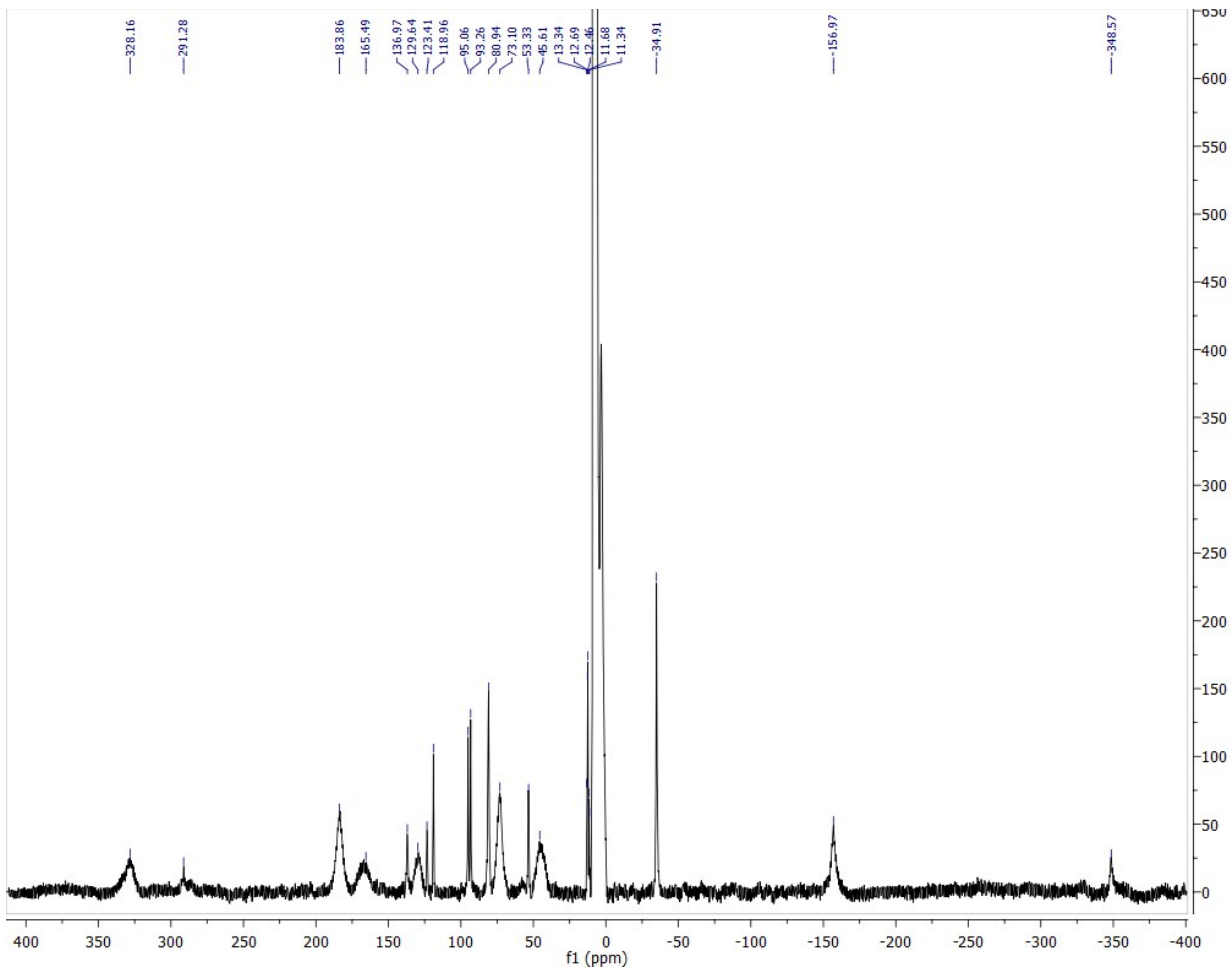


**Figure S2(a).** Baseline corrected  $^1\text{H}$  NMR (400 MHz) spectrum of **2** in  $\text{THF}-d_8$  at 25 °C.

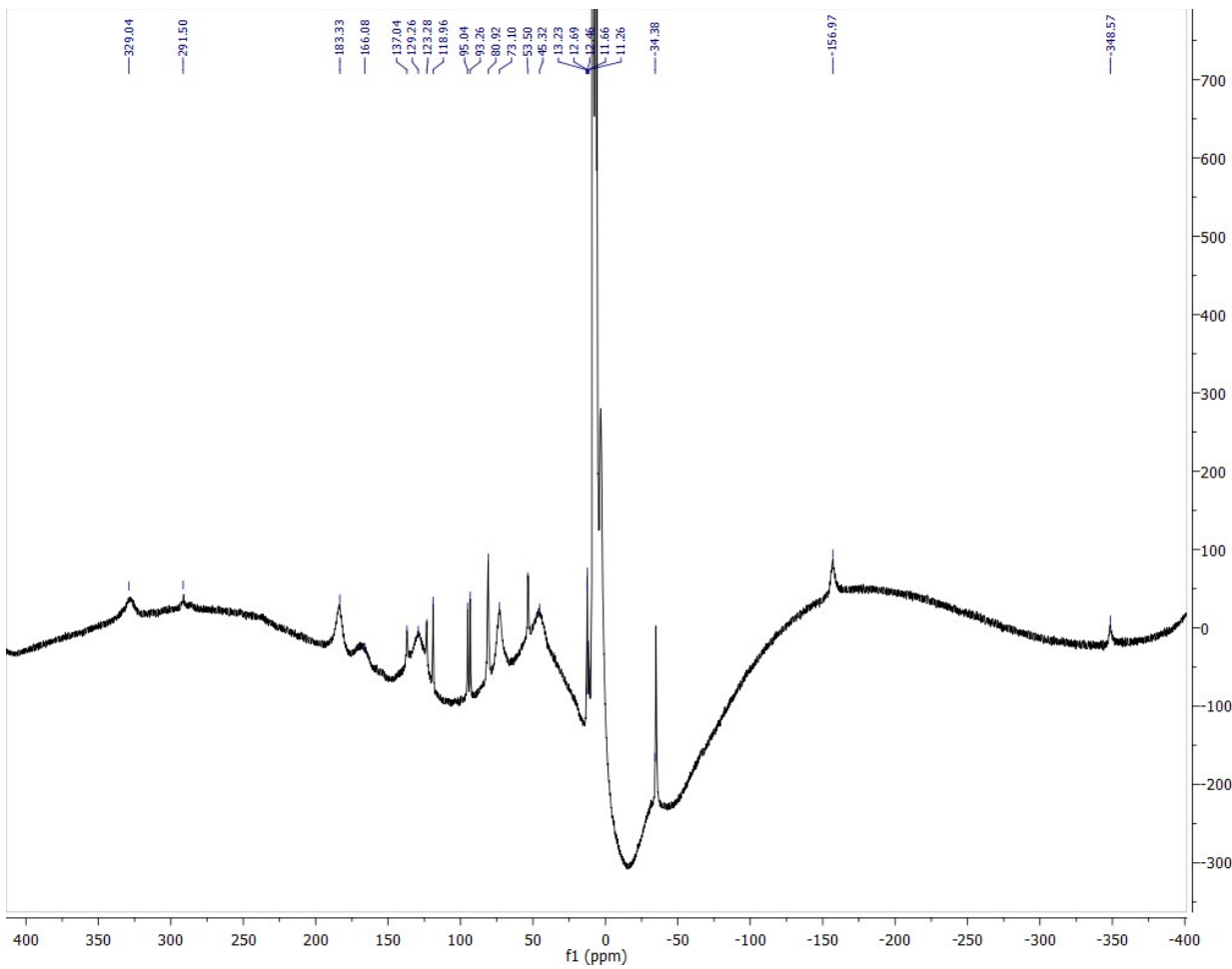


**Figure S2(b).** Baseline uncorrected <sup>1</sup>H NMR (400 MHz) spectrum of **2** in THF-*d*<sub>8</sub> at 25 °C

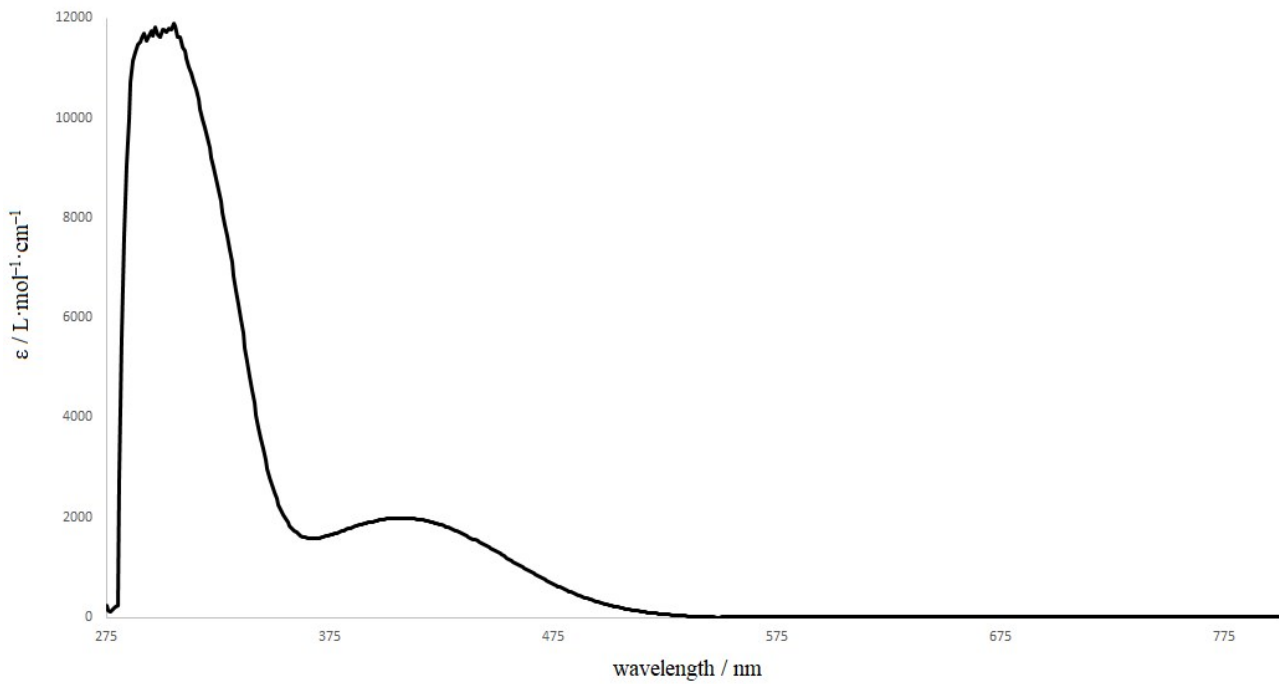


**Figure S3.** Room temperature electronic absorption spectrum of **1** (0.29mM in toluene).

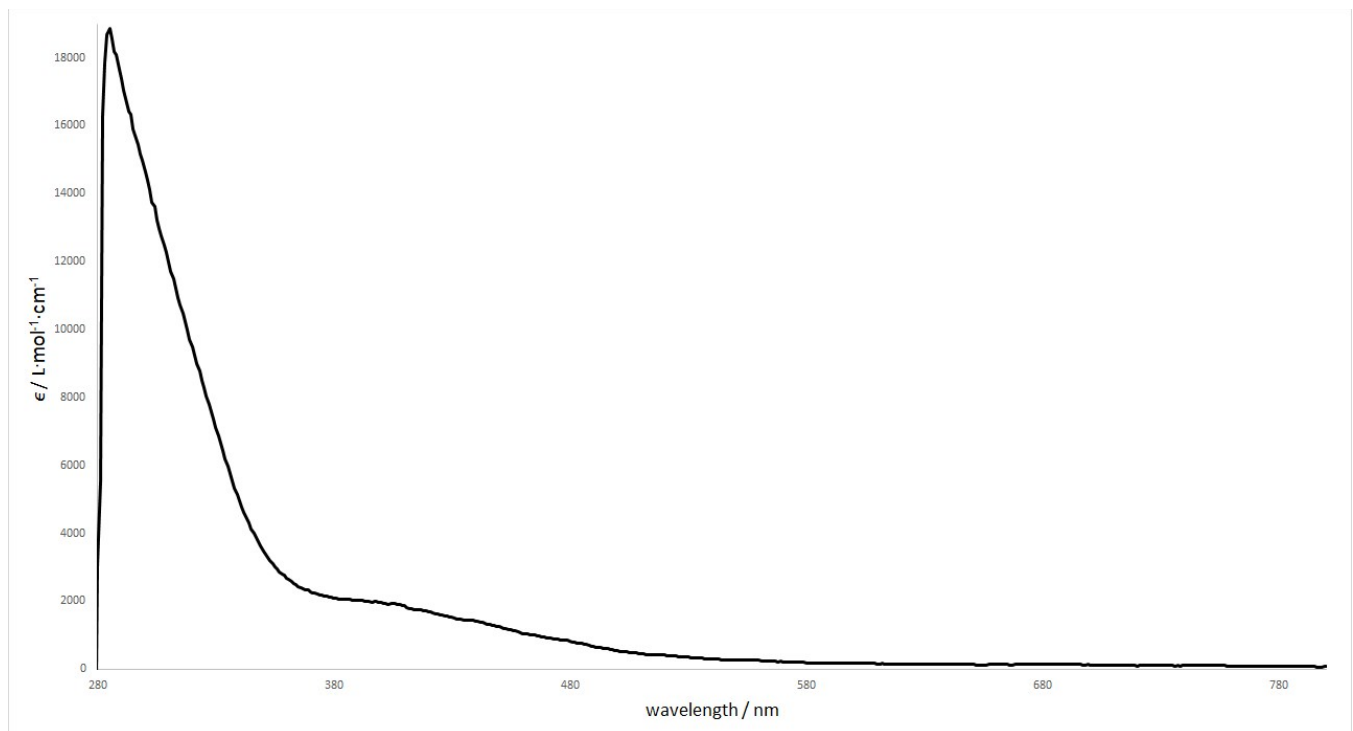


**Figure S4.** Room temperature electronic absorption spectrum of **2** (0.122 mM in toluene).

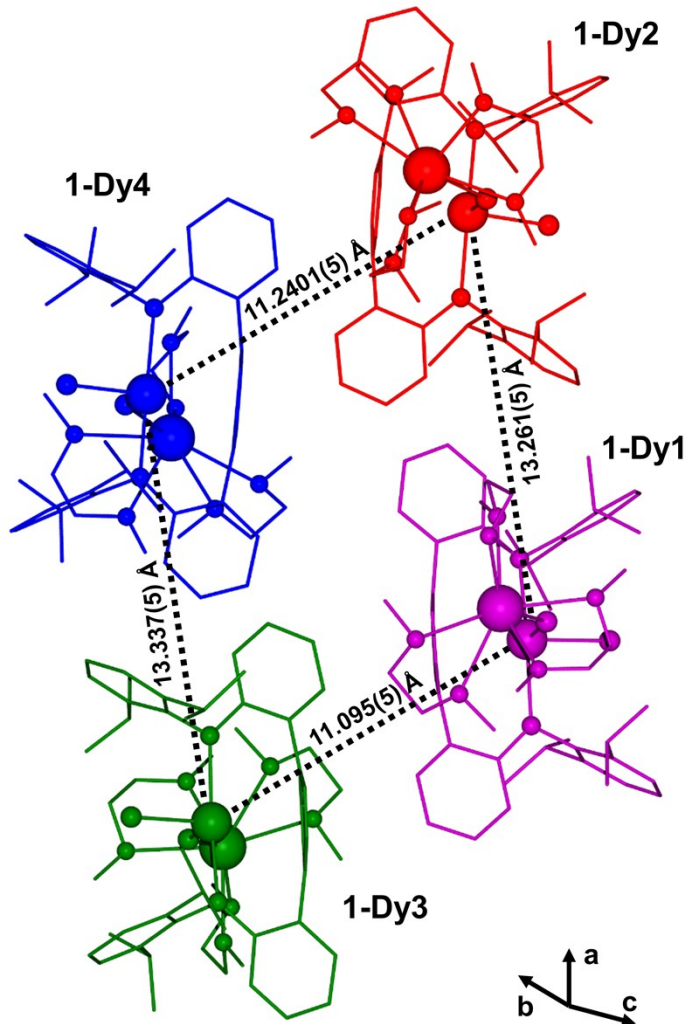


**Figure S5.** Four crystallographically independent molecules in the asymmetric unit of **1** (monoclinic *Pn*). Each of the independent molecules is depicted in a different colour; pink (**1-Dy1**), red (**1-Dy2**), green (**1-Dy3**), blue (**1-Dy4**). Protons have been omitted for clarity. Intermolecular Dy---Dy distances are represented by the black dotted lines, with the appropriate metrical data shown above the dotted lines.

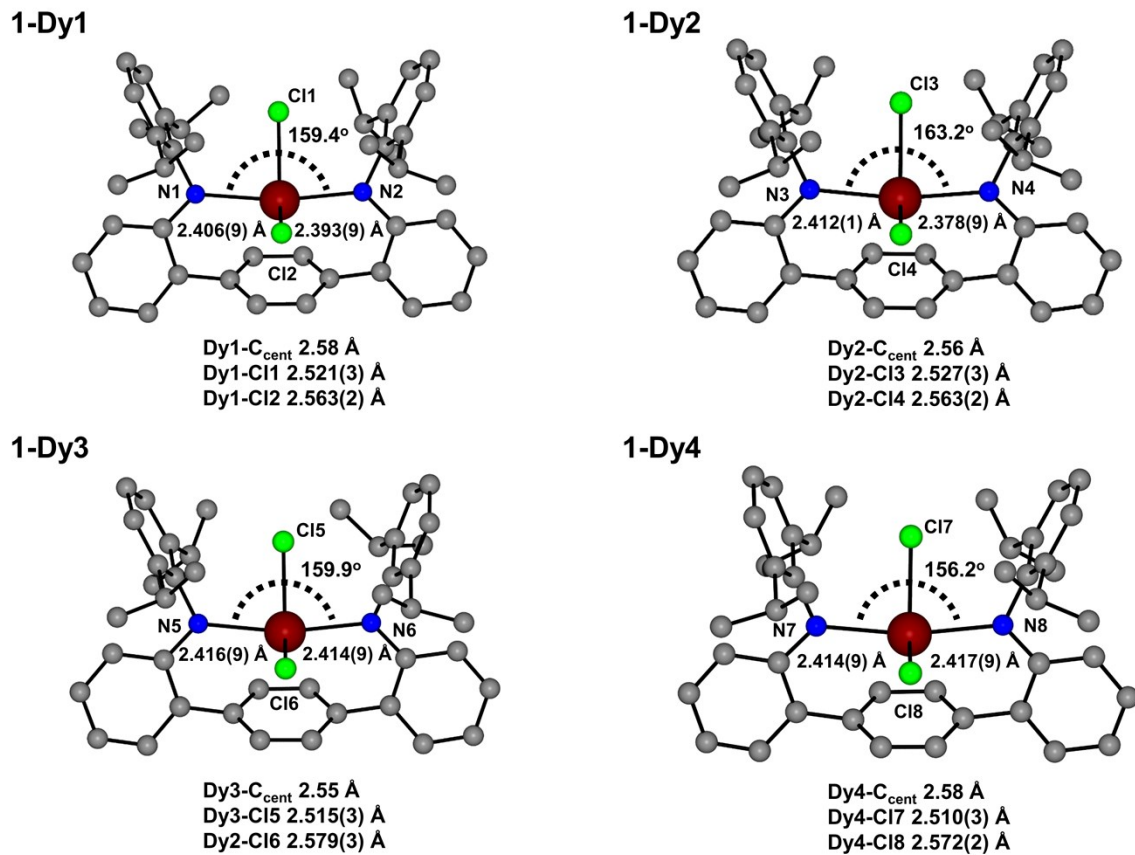


**Figure S6.** Solid-state molecular structure of the four crystallographically independent molecules (**1-Dy1**, **1-Dy2**, **1-Dy3**, **1-Dy4**) in the asymmetric unit of **1** (monoclinic *Pn*) collected under a He cryostream at 15 K. Protons and [K(DME)<sub>3</sub>] cations are removed for clarity. The dotted arch depicts the N-Dy-N angle, and the Dy-N distances are displayed below their representative bonds on the molecules. Dy-C<sub>cent</sub> and Dy-Cl distances are presented below the molecules.

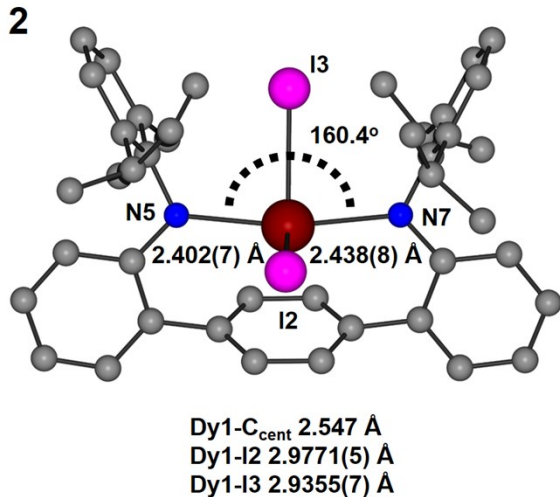


**Figure S7.** Solid-molecular structure of **2**. Protons and  $[\text{K}(\text{DME})_4]$  cation are removed for clarity. The dotted arch depicts the N-Dy-N angle, and the Dy-N distances are displayed below their representative bonds on the molecules. Dy-C<sub>cent</sub> and Dy-Cl distances are presented below the molecule.

**Details of the *Ab Initio* Calculations.** Electronic structure calculations were performed using MOLCAS-8.0 program<sup>[8]</sup> with the following basis set: Dy-ANO-RCC-VTZP; O and Cl, N- ANO-RCC-VDZP; C and H – ANO-RCC-VDZ.<sup>[9]</sup> Cholesky decomposition with the “high” accuracy threshold was used for the two electron integrals to speed up the calculation and reduce memory requirements.<sup>[10]</sup> Scalar relativistic effects were accounted using second order Douglas-Kroll-Hess approximation.<sup>[11]</sup> Active space for CASSCF<sup>[12]</sup> calculation of spin-free states consists of seven 4f orbitals with 9 electrons for Dy(III). Spin-orbit coupling was computed using the mean-field approximation<sup>[13]</sup> as implemented in RASSI. Molar magnetic susceptibility and magnetization were computed using SINGLE\_ANISO<sup>[14]</sup> routine together with the ligand field parameters for Stevens operator equivalence representation of the ground term with the total momentum  $J = 15/2$ .<sup>[15]</sup>

Calculations on two of the molecules in the asymmetric unit of **1** featuring the maximum (**1-Dy2**) and minimum (**1-Dy4**) N-Dy-N angles ( $163.18^\circ$  and  $156.25^\circ$ , respectively) show that the lowest KD is well isolated from the first excited state by  $323 \text{ cm}^{-1}$  (**1-Dy2**) and  $294 \text{ cm}^{-1}$  (**1-Dy4**), and its effective g-tensor is highly anisotropic;  $g'_z = 19.9567$  (**1-Dy2**) and  $g'_z = 19.8300$  (**1-Dy4**).

Comparatively, the calculations on the asymmetric unit of **2** also displays a well isolated ground state KD ( $2^{\text{nd}}$  KD = 337 cm $^{-1}$ ) which is also highly anisotropic ( $g_z' = 19.8300$ ). The orientation of the main magnetic axis is almost parallel to N-Dy-N bonds (*see Figure 1 in main text*). The nature of the wavefunction of the ground KD is 88% MJ=15/2 and 12% MJ=13/2.

**Table S2.** Energy splitting of the ground free ion  $J = 15/2$  multiplet and the effective g-tensors for the low-lying KDs for **1-Dy2**.

KD	Energy (cm $^{-1}$ )	g'1	g'2	g'3
<b>1</b>	0	0.0003	0.0002	19.9567
<b>2</b>	323	0.0138	0.0165	17.1339
<b>3</b>	630	0.1142	0.1363	14.2045
<b>4</b>	837	2.7977	6.161	8.9011
<b>5</b>	882	13.0964	3.9578	1.275
<b>6</b>	936	8.1422	10.3693	3.326
<b>7</b>	1000	15.9639	1.1859	0.4726
<b>8</b>	1120	0.0181	0.0981	19.0299

**Table S3.** Parameters of the crystal field acting on the ground  $J = 15/2$  multiple of **1-Dy2**.

q	K = 2	K = 4	K = 6
<b>-6</b>			0.86158469752200E-04
<b>-5</b>			-0.10633981818438E-03
<b>-4</b>		-0.91760884828230E-02	0.18642583169091E-04
<b>-3</b>		-0.14086244655349E-01	0.24224997515557E-03
<b>-2</b>	0.13759277070001E+01	-0.14285025336814E-02	-0.10245005043998E-04
<b>-1</b>	0.60568258227511E+01	0.20680347114299E-01	-0.23938258563324E-03
<b>0</b>	-0.55064478748947E+01	-0.70841322519724E-02	0.23586180988534E-04
<b>1</b>	0.41850561175636E+01	0.20734433397404E-01	-0.30055714833460E-03
<b>2</b>	-0.68657368182833E+00	0.10289683903598E-01	-0.10163342384825E-03
<b>3</b>		-0.14943562628113E-01	0.21065400387940E-05
<b>4</b>		-0.42423524791366E-02	-0.14861094420313E-04
<b>5</b>			0.37422404611554E-03
<b>6</b>			0.17707052063856E-03

**Table S4.** Energy splitting of the ground free ion  $J = 15/2$  multiplet and the effective g-tensors for the low-lying KDs for **1-Dy4**.

KD	Energy (cm <sup>-1</sup> )	g'1	g'2	g'3
<b>1</b>	0	19.8300	0.0003	0.0002
<b>2</b>	294	17.0367	0.0132	0.0156
<b>3</b>	567	14.1589	0.1233	0.1518
<b>4</b>	756	10.1002	1.9353	3.4765
<b>5</b>	789	17.9999	0.8381	0.1176
<b>6</b>	841	4.3763	11.3617	5.5460
<b>7</b>	884	14.7273	0.1488	0.9389
<b>8</b>	998	19.0753	0.0439	0.0198

**Table S5.** Parameters of the crystal field acting on the ground  $J = 15/2$  multiple of **1-Dy4**.

q	K = 2	K = 4	K = 6
<b>-6</b>			-0.79361156154741E-04
<b>-5</b>			-0.27267292140858E-04
<b>-4</b>		-0.30439108204695E-02	0.68422938523818E-04
<b>-3</b>		-0.18529487831441E-02	0.29869891007048E-04
<b>-2</b>	-0.79920811552959E-01	0.11198883196288E-01	-0.17417071280434E-03
<b>-1</b>	0.28599494401362E+00	0.18941683016905E-02	-0.31526907569805E-04
<b>0</b>	-0.52311665514918E+01	-0.74667826445692E-02	0.35836414935033E-04
<b>1</b>	0.11885846759185E+01	0.34272152433108E-02	-0.54142123313893E-04
<b>2</b>	0.13981371879997E+01	-0.12998660477119E-02	-0.38183385612794E-04
<b>3</b>		0.56607935416920E-03	-0.60463654159698E-05
<b>4</b>		0.12544729215488E-01	-0.47082382123324E-04
<b>5</b>			0.26440266706367E-04
<b>6</b>			0.18254608171442E-03

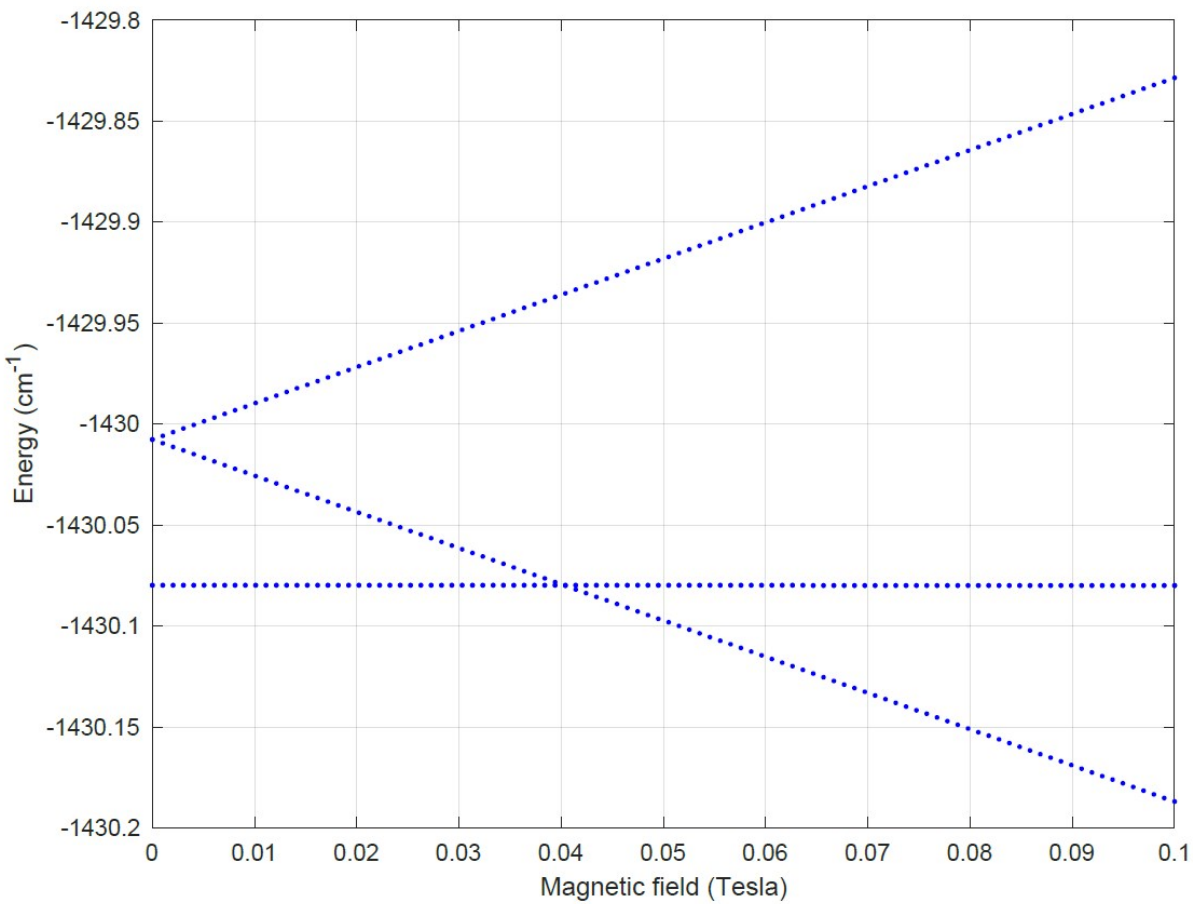


**Figure S8.** Four lowest states of two closest Dy complexes of **1** computed with Spinach 1.9 with account for dipolar coupling estimated based on LFT parameters from SINGLE\_ANISO and crystallographic positions with magnetic field applied along the main magnetic axis. The figure shows that magnetic field larger ~40 mT decouples dipolar interaction.

**Table S6.** Energy splitting of the ground free ion  $J = 15/2$  multiplet and the effective g-tensors for the low-lying KDs for **2**.

KD	Energy (cm <sup>-1</sup> )	g'1	g'2	g'3
<b>1</b>	0	19.883	0.0001	0.0001
<b>2</b>	337	17.0716	0.0106	0.0094
<b>3</b>	663	14.2201	0.0365	0.0279
<b>4</b>	906	11.1331	1.6501	1.3082
<b>5</b>	1028	12.3088	2.4631	3.5013
<b>6</b>	1051	0.9453	10.8352	3.7841
<b>7</b>	1089	1.9997	12.14865	6.1477
<b>8</b>	1173	18.714	0.3807	0.2456

**Table S7.** Parameters of the crystal field acting on the ground  $J = 15/2$  multiple of **2**.

q	K = 2	K = 4	K = 6
<b>-6</b>			-0.79361156154741E-04
<b>-5</b>			0.19242112830489E-03
<b>-4</b>		0.39880372896653E-02	-0.20432267401460E-04
<b>-3</b>		-0.26482342836212E-02	-0.87061230531053E-04
<b>-2</b>	0.16752865084159E+00	-0.90851456298114E-02	0.29821568924351E-04
<b>-1</b>	0.39646482700936E+00	-0.13738781928699E-02	0.15038172178457E-03
<b>0</b>	-0.66530092985073E+01	-0.71951245336476E-02	-0.81422340169123E-06
<b>1</b>	-0.44784204178090E+00	-0.31869352368885E-02	0.41048821195452E-04
<b>2</b>	0.11089368721060E+01	0.38389874398895E-02	0.37107631720323E-04
<b>3</b>		-0.23892900704950E-04	-0.11360069075366E-03
<b>4</b>		0.34016686935758E-02	-0.20689940768087E-04
<b>5</b>			0.23766420845702E-04
<b>6</b>			-0.74637611785098E-05

**Magnetic Measurements.** The magnetic susceptibility measurements were obtained using a Quantum Design SQUID magnetometer MPMS-XL7 operating between 1.8 and 300 K. DC measurements were performed on a polycrystalline sample of 17.0 mg for **1** and 23.0 mg for **2**. The samples were restrained with silicon grease and wrapped in a polyethylene membrane under an inert atmosphere. The samples were subjected to DC fields of -7 to 7 T, and a 3.78 Oe driving

field was used for AC measurements. The magnetization data were collected at 100 K to check for ferromagnetic impurities that were absent in both samples. Diamagnetic corrections were applied for the sample holder and the inherent diamagnetism of the samples were estimated with the use of Pascals constants.

#### DC Magnetism Plots for Compounds 1 and 2:

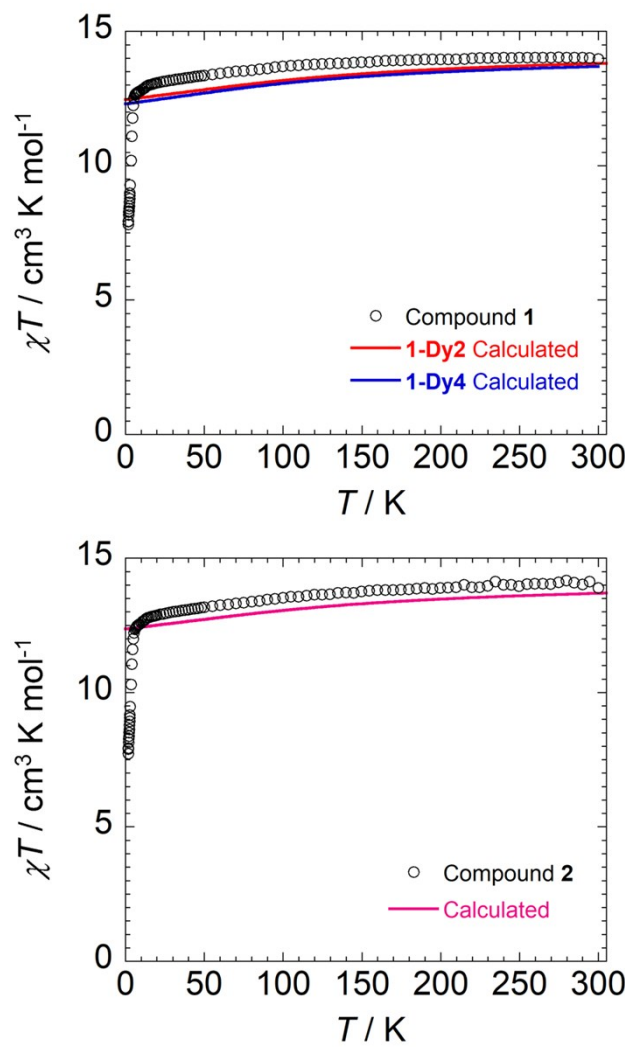


**Figure S9.** Temperature dependence of the  $\chi T$  product under an applied dc field of 1000 Oe for compound **1** (*top*) and compound **2** (*bottom*), where  $\chi$  is the molar magnetic susceptibility as defined by  $M/H$ . Experimental data is represented by black hollow circles. *Ab initio* calculated

magnetic susceptibility depicted by solid lines. For compound **1**, two of the four crystallographically independent molecules, **1-Dy2** (red) and **1-Dy4** (blue) which possess the upper and lower limits of the metrical data; N-Dy-N angles of  $162.3^\circ$  (**1-Dy2**) and  $156.2^\circ$  (**1-Dy4**) are modeled independently.

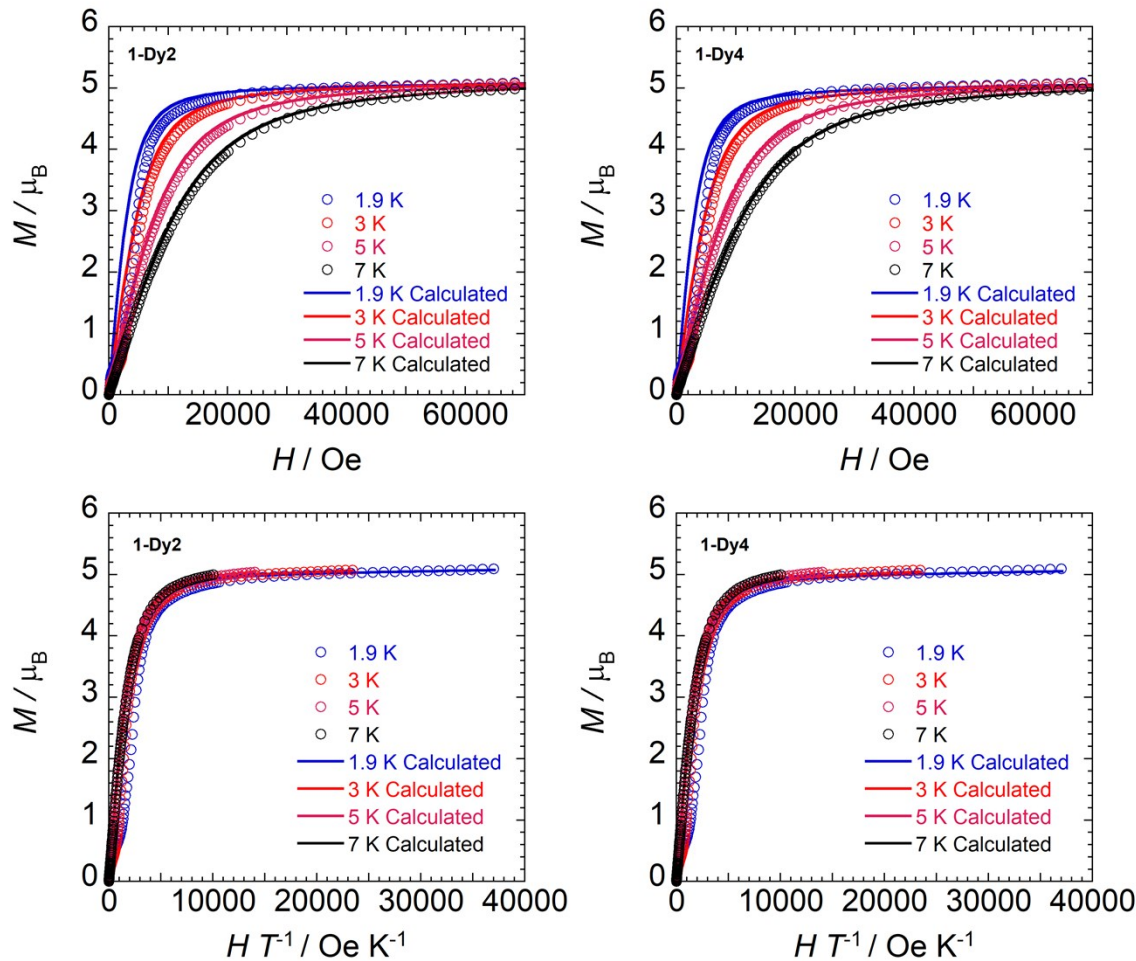


**Figure S10.** Solid state field dependence of the magnetization (*top*) and the reduced magnetization (*bottom*) for **1** at the indicated temperatures. Experimental data is represented by hollow circles and the calculated data represented by solid lines. Magnetization values calculated for two of the four crystallographically independent molecules (**1-Dy2** and **1-Dy4**) which possess the upper and lower limits of the metrical data; N-Dy-N angles of  $162.3^\circ$  (**1-Dy2**) and  $156.2^\circ$  (**1-Dy4**).

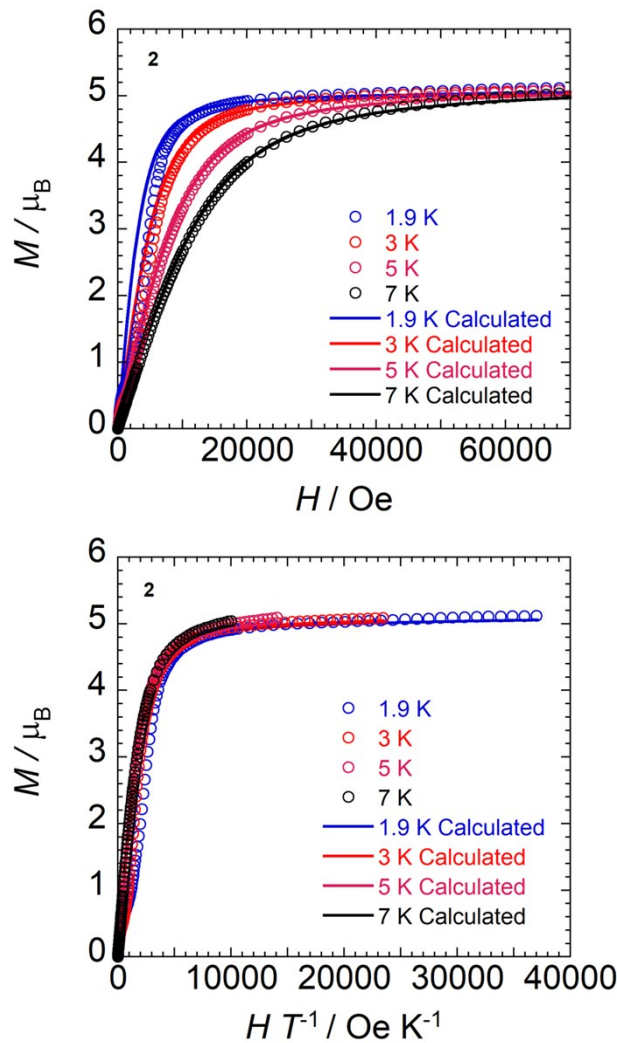


**Figure S11.** Solid state field dependence of the magnetization (*top*) and the reduced magnetization (*bottom*) for compound **2** at the indicated temperatures. Experimental data is represented by hollow circles and the calculated data represented by solid lines.

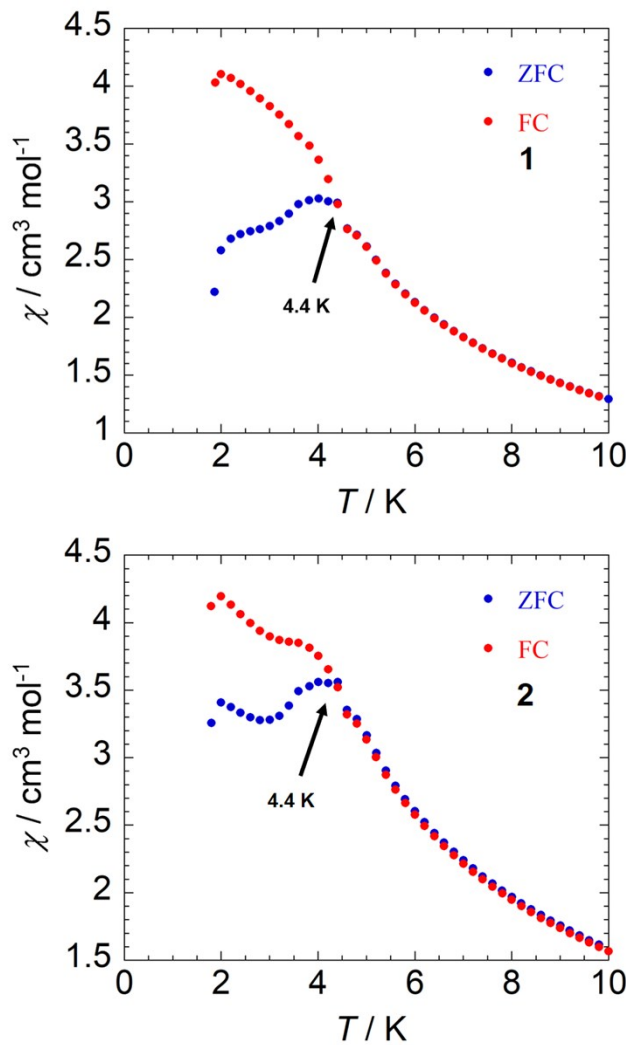


**Figure S12.** Zero-field-cooled and field-cooled (ZFC/FC) curves for **1** (*top*) and **2** (*bottom*) under an applied static field of 1000 Oe. Data were collected at a mean sweep rate of  $0.21 \text{ K min}^{-1}$ . ZFC and FC susceptibilities bifurcate at 4.4 K as indicated by the arrow in both samples.

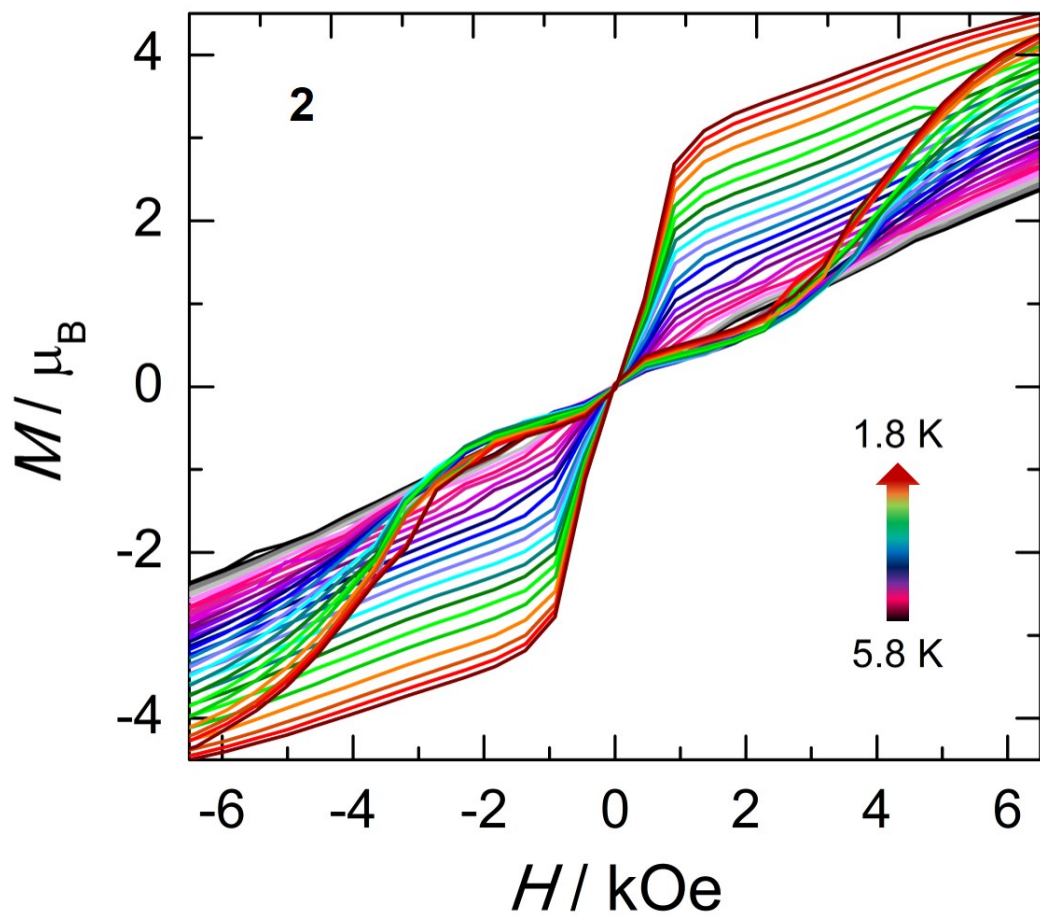


**Figure S13.** Magnetic hysteresis data for **2** in the temperature range 1.8-5.8 K. The measurement was completed by sweeping to  $H = 30$  kOe from  $H = 0$  Oe, and then cycling to  $H = -30$  kOe, and back to  $H = 30$  kOe. The average sweep rate was calculated at different field intervals, with a mean field sweep rate of  $12.2 \text{ Oe s}^{-1}$  over the entire data range (see Figure S14).

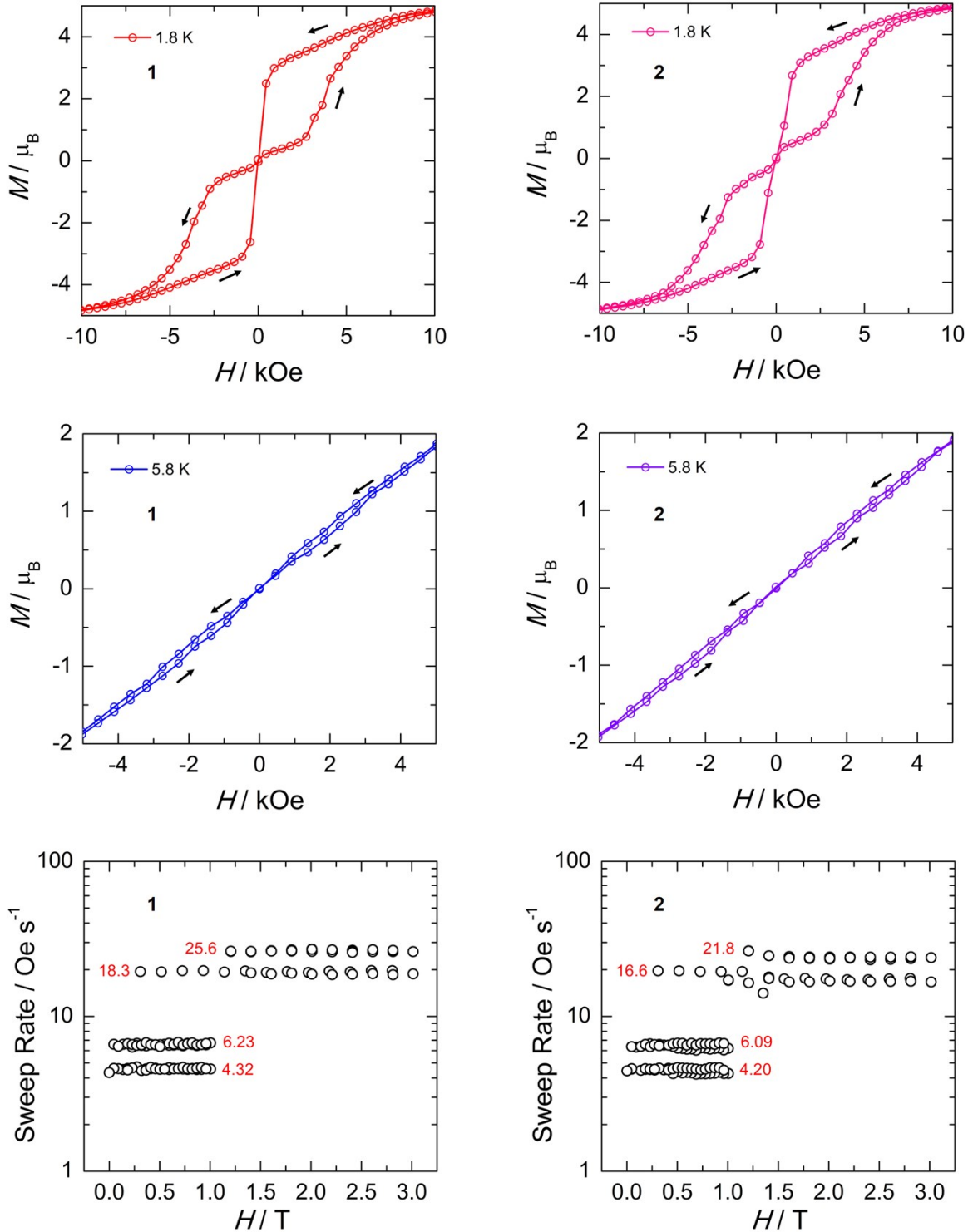


**Figure S14.** Magnetic hysteresis data for compound **1** (left) and compound **2** (right) at lowest measured temperature (1.8 K; *top*) and highest recorded temperature with openings  $H \neq 0$  Oe (5.8

K; *middle*). Black arrows indicate the direction of the field sweep. The average sweep rate was calculated at different field intervals (bottom), with a mean field sweep rate of  $13.6 \text{ Oe s}^{-1}$  (**1**) and  $12.2 \text{ Oe s}^{-1}$  (**2**) over the entire data range.

### AC Magnetism Plots for Compounds **1** and **2**:

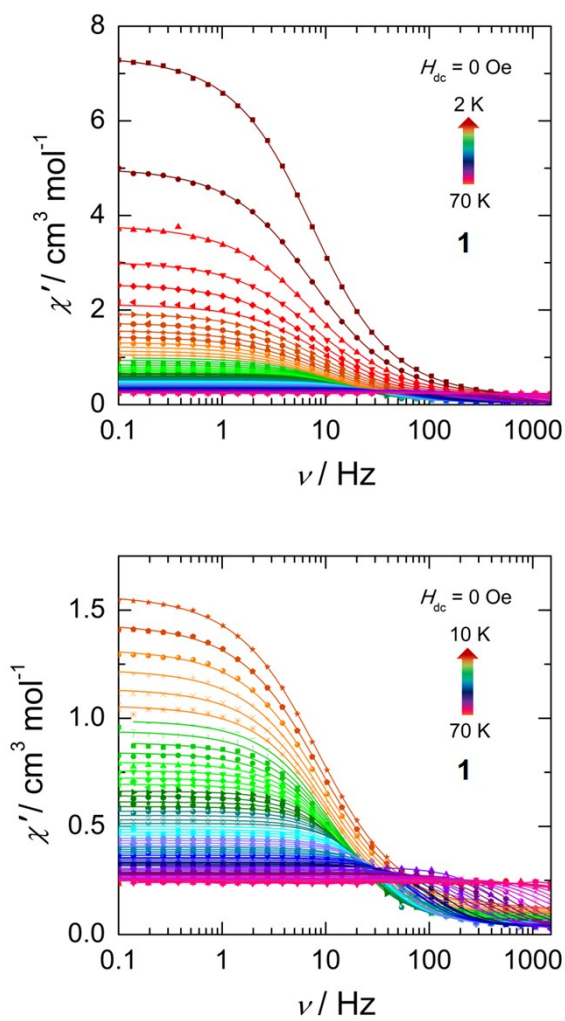


**Figure S15.** Frequency dependence of  $\chi'$  as a function of temperature in the range 2-70 K (*top*) and 10-70 K (*bottom*), in the absence of an applied static field ( $H_{\text{dc}} = 0 \text{ Oe}$ ) for compound **1**. Solid lines represent best fits to the generalized Debye model. Best fit parameters are summarized in Table S8.

**Table S8.** Best-fit parameters to the generalized Debye model for the frequency dependence of the in-phase magnetic susceptibility ( $\chi'$ ) as a function of temperature for **1** (Figure S15). Data collected in the absence of an applied static field ( $H_{dc} = 0$  Oe). Values in red were restrained in order to remain physically reasonable. Where no values were reported, no appropriate fit could be obtained.

T (K)	$\tau$ (s)	$\alpha$	$\chi_T$	$\chi_s$	$\chi_T - \chi_s$
2	0.02139	0.24325	7.38412	0.13765	7.24647
3	0.02121	0.25255	5.01681	0.15768	4.85914
4	0.02107	0.2541	3.80005	0.15905	3.64099
5	0.02022	0.24897	3.02868	0.15678	2.87189
6	0.0199	0.25574	2.55506	0.13921	2.41585
7	0.0179	0.22472	2.1229	0.14801	1.97489
8	0.01917	0.24989	1.93807	0.12002	1.81806
9	0.0189	0.25342	1.73522	0.11594	1.61928
10	0.01883	0.24989	1.57384	0.11156	1.46228
11	0.01844	0.24231	1.43889	0.10622	1.33267
12	0.01805	0.2339	1.32136	0.10629	1.21507
13	0.01749	0.22496	1.22732	0.09898	1.12834
14	0.01671	0.2111	1.13862	0.09409	1.04453
15	0.01569	0.19948	1.06045	0.09	0.97045
16	0.01505	0.17504	0.99105	0.0902	0.90085
17	0.01413	0.18506	0.94141	0.08195	0.85945
18	0.01328	0.17521	0.88915	0.08225	0.8069
19	0.01242	0.17056	0.84269	0.07705	0.76564
20	0.01155	0.1529	0.79758	0.07334	0.72424
21	0.01121	0.11967	0.75741	0.0781	0.6793
22	0.01027	0.1297	0.72519	0.07423	0.65095
23	0.00965	0.11377	0.69534	0.07186	0.62347
24	0.00923	0.08319	0.66314	0.06908	0.59407
25	0.00832	0.11306	0.64164	0.06019	0.58144
26	0.00787	0.08338	0.61364	0.06101	0.55263
27	0.00727	0.07365	0.59176	0.05875	0.53301
28	0.00693	0.06239	0.57021	0.06084	0.50937
29	0.00651	0.05356	0.55071	0.05993	0.49077
30	0.00585	0.05718	0.53064	0.05547	0.47517
31	0.00554	0.03004	0.51365	0.05896	0.45469
32	0.00531	0.04867	0.50008	0.05696	0.44312
33	0.00501	0.04905	0.4857	0.05379	0.43192
34	0.00472	0.04175	0.47365	0.05395	0.4197
35	0.00435	0.04381	0.45959	0.05276	0.40682
36	0.00403	0.0434	0.44481	0.0494	0.39541

37	0.00391	0.03419	0.43408	0.04748	0.3866
38	0.00334	0.02527	0.42178	0.04319	0.37859
39	0.00323	0.0108	0.41018	0.04799	0.3622
40	0.00312	0.04671	0.40303	0.04541	0.35763
41	0.00283	0.03866	0.39315	0.0441	0.34905
42	0.0028	0.03921	0.38424	0.04497	0.33927
43	0.00245	0.02992	0.37518	0.04256	0.33262
44	0.00237	0.02154	0.36627	0.04532	0.32094
45	0.00216	0	0.35595	0.04181	0.31414
46	0.00195	0.04152	0.35279	0.0331	0.3197
47	0.0019	0.02757	0.34405	0.03763	0.30641
48	0.00164	0	0.33503	0.04003	0.295
49	0.00156	0.03054	0.33036	0.03507	0.29528
50	0.00147	0.01044	0.3242	0.03881	0.28539
51	0.00117	0.00838	0.31804	0.0368	0.28124
52	3.48E-04	0.04879	0.31203	0.01947	0.29256
53	9.06E-04	0.02962	0.30593	0.04025	0.26568
54	7.24E-04	0.00302	0.29898	0.02892	0.27006
55	5.64E-04	0.05994	0.29779	0.01399	0.2838
56	5.14E-04	0.04773	0.29048	0.03102	0.25946
57	4.01E-04	0.05188	0.28469	0.02485	0.25983
58	3.33E-04	0	0.28045	0.03232	0.24813
59	2.53E-04	0	0.27647	0.03094	0.24552
60	1.90E-04	0.01163	0.27064	0.01679	0.25385
61	1.37E-04	0.07916	0.26823	0.0099	0.25833
62	1.30E-04	0.03436	0.26196	0.05525	0.20671
63	8.06E-05	0.05259	0.2597	0	0.2597
64	6.96E-05	0	0.25444	0	0.25444
65	5.51E-05	0.04532	0.25212	0.03152	0.2206
66	1.31E-04	0	0.24822	0.19353	0.05469
67	2.67E-05	0.04167	0.24281	0	0.24281
68	2.21E-05	0.08819	0.24025	0	0.24025
69	--	--	--	--	--
70	--	--	--	--	--

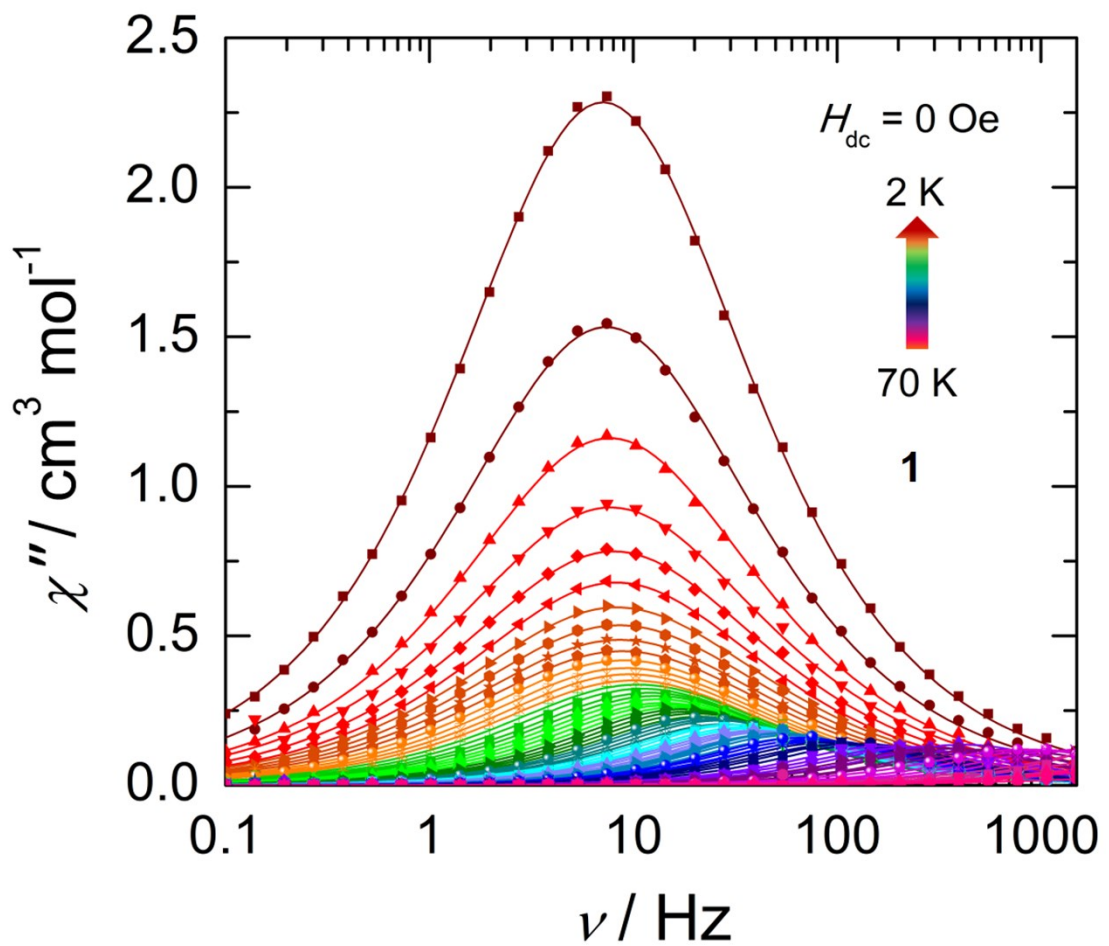


**Figure S16.** Frequency dependence of  $\chi''$  as a function of temperature in the range 2-70 K, in the absence of an applied static field ( $H_{dc} = 0$  Oe) for compound **1**. Solid lines represent best fits to the generalized Debye model. Best fit parameters are summarized in Table S9.

**Table S9.** Best-fit parameters to the generalized Debye model for the frequency dependence of the out-of-phase magnetic susceptibility ( $\chi''$ ) as a function of temperature for **1** (Figure 4c and S16). Data collected in the absence of an applied static field ( $H_{dc} = 0$  Oe). Values in red were restrained in order to remain physically reasonable.

T (K)	$\tau$ (s)	$\alpha$	$\chi_T$	$\chi_s$	$\chi_T - \chi_s$
2	0.02238	0.2413	6.75939	0.02131	6.73808
3	0.02155	0.24513	4.55277	0.00221	4.55056
4	0.02074	0.24347	3.51801	0.08003	3.43798
5	0.02048	0.26031	2.83471	0.00301	2.8317
6	0.01984	0.25447	3.27772	0.91733	2.36039
7	0.01927	0.24528	2.01627	0.00224	2.01403
8	0.01912	0.25462	1.8062	0.01065	1.79555
9	0.01866	0.25329	1.64269	0.03099	1.61169
10	0.01846	0.24947	1.52934	0.07452	1.45481
11	0.01804	0.24407	1.32988	4.55E-04	1.32942
12	0.01774	0.23166	1.23756	0.02433	1.21322
13	0.01715	0.22254	1.12591	0.0051	1.1208
14	0.01658	0.21148	1.04627	0.00439	1.04188
15	0.01606	0.20352	0.97147	0.00103	0.97044
16	0.01502	0.19244	0.98226	0.06655	0.91571
17	0.01433	0.17586	0.88801	0.03382	0.8542
18	0.01319	0.16878	0.81989	0.01038	0.8095
19	0.01239	0.16278	0.84454	0.0712	0.77335
20	0.01189	0.14573	0.72708	0.00231	0.72476
21	0.01131	0.13799	0.70072	0.01514	0.68559
22	0.0105	0.12696	0.68367	0.0265	0.65717
23	0.00976	0.11412	0.91076	0.28608	0.62468
24	0.00913	0.10517	0.80193	0.20098	0.60095
25	0.00862	0.09159	0.58474	0.01563	0.56911
26	0.00787	0.09408	0.56548	0.00897	0.55651
27	0.00749	0.0876	0.53628	0.00902	0.52727
28	0.007	0.07713	0.51898	0.00728	0.5117
29	0.00656	0.07266	0.49703	0.0032	0.49383
30	0.00606	0.06079	0.47828	0.00104	0.47724
31	0.0057	0.07043	0.45714	4.41E-04	0.4567
32	0.00529	0.06624	0.46105	0.01032	0.45073
33	0.00498	0.0425	0.45044	0.01769	0.43275
34	0.00456	0.04954	0.42494	0.00518	0.41976
35	0.00421	0.05887	0.42317	0.00675	0.41643
36	0.00405	0.06339	0.40488	0.00117	0.40371

37	0.00389	0.0493	0.38512	7.32E-06	0.38512
38	0.00356	0.03107	0.37496	0.00118	0.37378
39	0.00343	0.05129	0.36388	1.30E-04	0.36375
40	0.00315	0.02408	0.35982	2.98E-04	0.35952
41	0.00298	0.00212	0.35157	8.75E-04	0.35069
42	0.00278	0.02228	0.35174	0.00577	0.34597
43	0.00255	0.03335	0.33842	0.00695	0.33147
44	0.00238	0.01557	0.33582	0.01044	0.32537
45	0.00217	0.03954	0.33628	0.01285	0.32343
46	0.00195	0.03737	0.32694	0.01565	0.31128
47	0.00188	0.00848	0.31976	0.01478	0.30498
48	0.00172	0.01969	0.31378	0.01646	0.29732
49	0.00149	0.03879	0.31574	0.02205	0.29369
50	0.00135	0.01448	0.3068	0.02227	0.28453
51	0.00114	0	0.30167	0.02713	0.27454
52	3.86E-04	0.02559	0.31996	0.03688	0.28309
53	9.21E-04	0	0.29448	0.03121	0.26327
54	7.47E-04	0.03703	0.29615	0.03156	0.26459
55	6.23E-04	0.00718	0.29551	0.03508	0.26043
56	5.02E-04	0.02555	0.30669	0.04715	0.25954
57	4.27E-04	0	0.2855	0.04016	0.24534
58	3.16E-04	0	0.28373	0.04474	0.239
59	2.39E-04	0.06518	0.30727	0.04458	0.26268
60	1.87E-04	0.0519	0.30647	0.04647	0.26
61	1.57E-04	0	0.28839	0.05257	0.23583
62	1.20E-04	0	0.28477	0.05162	0.23315
63	8.54E-05	0	0.28984	0.04164	0.24819
64	2.83E-05	0.14604	0.41594	0	0.41594
65	3.63E-06	0.05947	2.5811	0	2.5811
66	7.04E-05	0	0.16127	0	0.16127
67	3.45E-05	0.1433	0.18932	0	0.18932
68	3.46E-06	0.14389	1.03257	0	1.03257
69	2.74E-06	0.03303	1.03976	0	1.03976
70	9.17E-06	0.28601	0.15733	0	0.15733

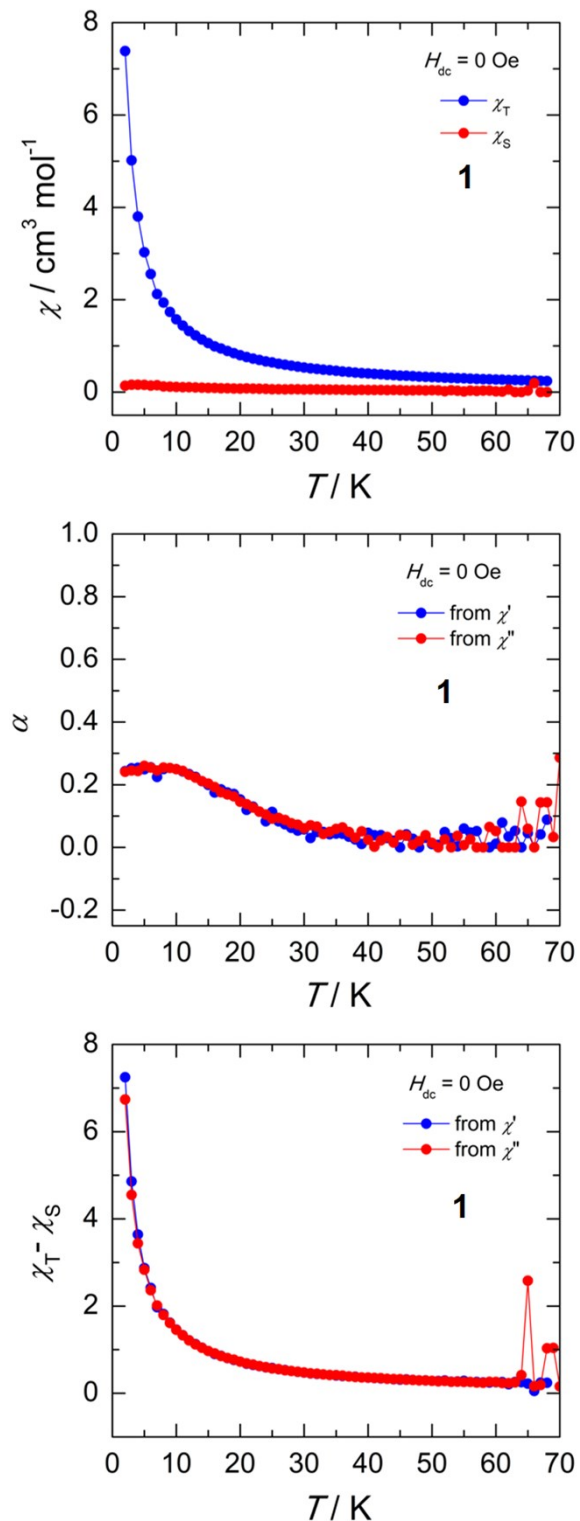


**Figure S17.** Data obtained from the generalized Debye fits of  $\chi'$  and  $\chi''$  frequency dependent ac data collected in the absence of an applied static field ( $H_{dc} = 0$  Oe) for compound **1**. Temperature dependence of  $\chi_T$  and  $\chi_S$  (top),  $\alpha$  (middle), and  $\chi_T - \chi_S$  (bottom).

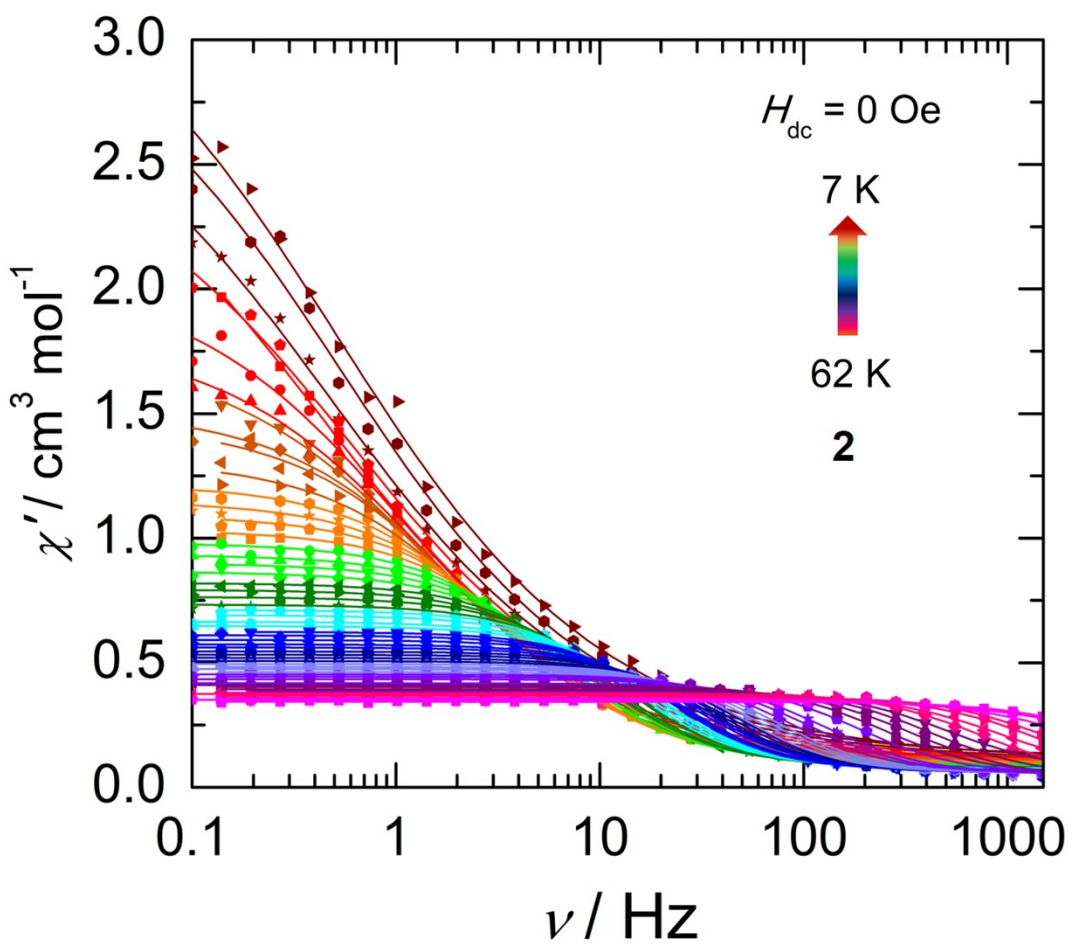


**Figure S18.** Frequency dependence of  $\chi'$  as a function of temperature in the range 7-62 K, in the absence of an applied static field ( $H_{\text{dc}} = 0$  Oe) for compound **2**. Solid lines represent best fits to the generalized Debye model. Best fit parameters are summarized in Table S10.

**Table S10.** Best-fit parameters to the generalized Debye model for the frequency dependence of the in-phase magnetic susceptibility ( $\chi'$ ) as a function of temperature for **2** (Figure S18). Data collected in the absence of an applied static field ( $H_{dc} = 0$  Oe). Values in red were restrained in order to remain physically reasonable. Where no values were reported, no appropriate fit could be obtained.

T (K)	$\tau$ (s)	$\alpha$	$\chi_s$	$\chi_T$	$\chi_T - \chi_s$
7	0.31157	0.46024	0.10201	3.5282	3.42619
8	0.29831	0.43804	0.11371	3.24019	3.12647
9	0.34386	0.45871	0.0996	3.04995	2.95035
10	0.26134	0.43755	0.1001	2.64796	2.54786
11	0.37007	0.45516	0.08672	2.88594	2.79921
12	0.15644	0.36907	0.10725	2.07813	1.97088
13	0.12027	0.34803	0.10479	1.82294	1.71815
14	0.11376	0.34295	0.09785	1.75984	1.66199
15	0.08033	0.28139	0.10742	1.5234	1.41599
16	0.07365	0.27081	0.10124	1.47025	1.36901
17	0.05896	0.24134	0.10263	1.31904	1.21641
18	0.04867	0.21714	0.09909	1.2221	1.12301
19	0.04197	0.20363	0.09155	1.15241	1.06087
20	0.03721	0.18196	0.09653	1.09378	0.99725
21	0.03207	0.17012	0.08928	1.03547	0.94619
22	0.02795	0.1573	0.08943	0.98213	0.8927
23	0.02463	0.13847	0.08754	0.93398	0.84644
24	0.02178	0.14756	0.08327	0.90142	0.81815
25	0.01893	0.1518	0.07548	0.86617	0.79069
26	0.01724	0.11309	0.08013	0.82119	0.74106
27	0.01552	0.11455	0.07573	0.79373	0.71799
28	0.01333	0.10865	0.07491	0.76436	0.68945
29	0.01226	0.09611	0.07365	0.73386	0.66021
30	0.01117	0.08677	0.07544	0.71229	0.63685
31	0.0102	0.09147	0.07399	0.69179	0.6178
32	0.00889	0.08382	0.06859	0.66445	0.59586
33	0.00824	0.08512	0.06731	0.64756	0.58025
34	0.00735	0.07733	0.06466	0.6243	0.55964
35	0.00694	0.07719	0.06885	0.61049	0.54164
36	0.00635	0.06175	0.06804	0.59188	0.52384
37	0.00558	0.07275	0.06508	0.57368	0.5086
38	0.00504	0.07653	0.05731	0.56131	0.504
39	0.00471	0.06159	0.06533	0.5453	0.47997
40	0.00425	0.05569	0.06033	0.53221	0.47188

41	0.00388	0.06715	0.05903	0.51978	0.46075
42	0.00347	0.05676	0.06013	0.50699	0.44686
43	0.0032	0.04334	0.05938	0.49506	0.43569
44	0.00279	0.05122	0.06068	0.48399	0.42331
45	0.00243	0.06046	0.05413	0.47417	0.42004
46	0.00213	0.0519	0.05423	0.46268	0.40846
47	0.00185	0.05157	0.05973	0.45306	0.39334
48	0.0015	0.05846	0.05256	0.44376	0.3912
49	0.00127	0.05302	0.05399	0.4341	0.38011
50	--	--	--	--	--
51	8.56798E-4	0.05476	0.05327	0.41763	0.36436
52	6.54277E-4	0.06415	0.0518	0.41088	0.35908
53	4.67543E-4	0.0912	0.03142	0.40287	0.37145
54	3.7646E-4	0.07398	0.04371	0.3935	0.3498
55	3.12834E-4	0.079	0.06443	0.38826	0.32383
56	2.16697E-4	0.08112	0.04073	0.37997	0.33924
57	1.70931E-4	0.10597	0.04967	0.3748	0.32513
58	1.02974E-4	0.11897	0	0.36815	0.36815
59	1.2877E-4	0.01464	0.11045	0.35859	0.24814
60	5.66069E-5	0.15821	0	0.35561	0.35561
61	4.77069E-5	0.21925	0.09026	0.35135	0.26109
62	4.27954E-5	0.10442	0.04577	0.34314	0.29737

**Table S11.** Best-fit parameters to the generalized Debye model for the frequency dependence of the out-of-phase magnetic susceptibility ( $\chi''$ ) as a function of temperature for **2** (Figure 4d). Data collected in the absence of an applied static field ( $H_{dc} = 0$  Oe). Values in red were restrained in order to remain physically reasonable. Where no values were reported, no appropriate fit could be obtained.

T (K)	$\tau$ (s)	$\alpha$	$\chi_s$	$\chi_T$	$\chi_T - \chi_s$
7	0.30506	0.33581	0.00653	2.84687	2.84034
8	0.29184	0.36316	0.00486	2.65529	2.65044
9	0.22301	0.24866	0.02781	2.0487	2.02089
10	0.19835	0.24045	0.00275	1.84358	1.84083
11	0.16799	0.22122	0.02614	1.70542	1.67928
12	0.13695	0.18788	0.00721	1.51485	1.50764
13	0.12296	0.15371	0.00595	1.36356	1.35761
14	0.09802	0.16316	0.01509	1.30081	1.28571
15	0.0841	0.1541	8.05216E-4	1.21487	1.21406
16	0.07235	0.13965	0.14111	1.27475	1.13364
17	0.06086	0.12236	4.71194E-4	1.06253	1.06206
18	0.05242	0.1237	0.04274	1.05788	1.01513
19	0.04495	0.12279	2.54706E-5	0.97011	0.97008
20	0.03696	0.16941	0.00893	0.98833	0.9794
21	0.03261	0.15625	0.0852	1.01375	0.92854
22	0.03009	0.09916	1.06462E-4	0.84118	0.84107
23	0.02556	0.12507	0.02062	0.85243	0.83181
24	0.02232	0.13496	0.00466	0.81025	0.8056
25	0.02013	0.11639	0.00109	0.76625	0.76516
26	0.01773	0.11141	0.04611	0.78558	0.73947
27	0.01557	0.10494	2.25134E-4	0.71637	0.71615
28	0.01392	0.12177	0.00991	0.69936	0.68946
29	0.01255	0.10131	2.93435E-4	0.66345	0.66316
30	0.01112	0.09778	0.02688	0.66627	0.63939
31	0.01025	0.08315	1.73172E-4	0.61446	0.61429
32	0.00934	0.09233	2.76566E-4	0.60007	0.59979
33	0.00821	0.09292	0.00757	0.59274	0.58517
34	0.00739	0.09853	3.90787E-4	0.57141	0.57102
35	0.00678	0.08654	5.13499E-4	0.55084	0.55032
36	0.00619	0.08734	0.00787	0.54274	0.53487
37	0.00567	0.08715	0.00201	0.52057	0.51856
38	0.00504	0.0832	1.29986E-4	0.50935	0.50922
39	0.00472	0.06973	2.51064E-4	0.48758	0.48733
40	0.00425	0.07807	3.64101E-4	0.47978	0.47941

41	0.00383	0.08005	0.01212	0.47955	0.46742
42	0.00353	0.06172	4.11503E-4	0.44972	0.44931
43	0.00314	0.0692	0.00711	0.44815	0.44103
44	0.0028	0.05628	1.35965E-4	0.43458	0.43445
45	0.00241	0.08045	8.00308E-5	0.43138	0.4313
46	0.00207	0.0495	0.00224	0.40458	0.40235
47	0.00182	0.07533	9.57389E-5	0.40512	0.40503
48	0.00153	0.07047	2.85837E-4	0.39946	0.39917
49	0.00132	0.04866	1.52392E-5	0.38015	0.38013
50	--	--	--	--	--
51	8.10442E-4	0.07266	0.00342	0.3798	0.37637
52	6.63318E-4	0.05172	0.00136	0.35897	0.35761
53	4.71416E-4	0.1089	0.00182	0.37383	0.37202
54	3.75823E-4	0.07582	0.0052	0.35637	0.35117
55	2.72585E-4	0.09267	0.0024	0.35616	0.35375
56	2.21506E-4	0.08818	4.32447E-4	0.33405	0.33361
57	1.68762E-4	0.08645	0.00229	0.3345	0.33221
58	1.19462E-4	0.10677	0.01254	0.35972	0.34718
59	8.94756E-5	0.14529	0.02636	0.36321	0.33685
60	5.30402E-5	0.17792	0.00642	0.38134	0.37491
61	4.08513E-5	0.18673	0.01095	0.37882	0.36787
62	4.38583E-6	0.2404	0	1.29304	1.29304

**Table S12.** Best-fit parameters to the generalized Debye model for the frequency dependence of the out-of-phase magnetic susceptibility ( $\chi''$ ) as a function of field for **1** collected at  $T = 20$  K (Figure 4a).

H (Oe)	$\tau$ (s)	$\alpha$	$\chi_T$	$\chi_s$	$\chi_T - \chi_s$
0	0.01216	0.12817	0.79372	0.0023	0.79142
50	0.01235	0.14688	0.82144	0.01519	0.80625
100	0.01629	0.18952	0.80867	2.93E-04	0.80838
150	0.02543	0.19983	0.80406	0.00136	0.80271
200	0.03694	0.17607	0.80448	0.00151	0.80297
250	0.04763	0.12146	0.8117	0.02067	0.79103
300	0.05459	0.08505	0.79575	6.93E-04	0.79506
350	0.06225	0.06034	0.79004	6.21E-05	0.78998
400	0.06584	0.03971	1.08814	0.29936	0.78878
600	0.07243	0.01577	0.79574	6.42E-04	0.79509
800	0.07406	0.00534	0.7947	0.00232	0.79238
1000	0.07426	0.01016	0.7989	9.81E-05	0.7988
1200	0.07509	0.0039	0.90047	0.10525	0.79522
1400	0.07501	0.00768	0.7997	0.00232	0.79737
1600	0.07429	0	0.78896	5.88E-04	0.78837
1800	0.07488	0.01216	0.80222	2.07E-05	0.8022
2000	0.07448	0.01449	0.8052	0.00309	0.80211
2200	0.07557	0.01054	0.90106	0.10215	0.79891
2400	0.07498	0.00381	0.79352	4.11E-05	0.79348
2600	0.07391	0.00918	0.80312	0.00502	0.7981
2800	0.07335	0.00545	0.79874	5.46E-04	0.79819
3000	0.07377	0.00299	0.79447	0.00253	0.79194
3500	0.07358	4.86E-04	0.79137	0.00176	0.78961
4000	0.07285	0.00312	0.79603	0.00778	0.78825
4500	0.07157	0.0031	0.78947	7.07E-05	0.7894
5000	0.07038	0.00451	0.8508	0.06117	0.78963

**Table S13.** Best fit parameters to the generalized Debye model for the frequency dependence of the out-of-phase ( $\chi''$ ) magnetic susceptibility as a function of field for **2** collected at  $T = 20$  K (Figure 4b).

H (Oe)	$\tau$ (s)	$\alpha$	$\chi_s$	$\chi_T$	$\chi_T - \chi_s$
0	0.03476	0.17942	7.63057E-4	0.87145	0.87068
50	0.03467	0.18781	0.11738	0.99756	0.88018
100	0.03525	0.18237	0.00783	0.88122	0.87339
150	0.03566	0.17722	0.00314	0.86964	0.8665
200	0.03666	0.18901	1.24065E-4	0.87069	0.87057
250	0.03705	0.21598	0.00106	0.89175	0.89068
300	0.03875	0.22578	0.00464	0.89942	0.89478
350	0.0418	0.22782	0.00135	0.89607	0.89472
400	0.04646	0.2341	0.00831	0.90513	0.89682
600	0.06426	0.1863	0.00103	0.88326	0.88223
800	0.07585	0.1489	0.13655	1.00721	0.87066
1000	0.07788	0.17369	4.60366E-4	0.86	0.85954
1200	0.08402	0.11955	0.0325	0.90165	0.86915
1400	0.08486	0.11816	0.05125	0.92496	0.87371
1600	0.0867	0.10279	0.10923	0.97134	0.86211
1800	0.08646	0.11255	0.08085	0.95294	0.87209
2000	0.08656	0.10837	0.00132	0.87067	0.86935
2200	0.08696	0.10751	2.72535E-4	0.86884	0.86857
2400	0.08694	0.10547	1.93501E-4	0.86994	0.86974
2600	0.08779	0.11616	1.22114E-4	0.87915	0.87903
2800	0.08565	0.09829	0.00157	0.86156	0.85999
3000	0.08238	0.08309	2.79763E-4	0.84243	0.84215
3500	0.0851	0.10649	0.00375	0.8693	0.86554
4000	0.08494	0.10586	3.91296E-4	0.86379	0.8634
4500	0.08363	0.09879	0.0519	0.90664	0.85474
5000	0.08696	0.14344	0.02026	0.91669	0.89643

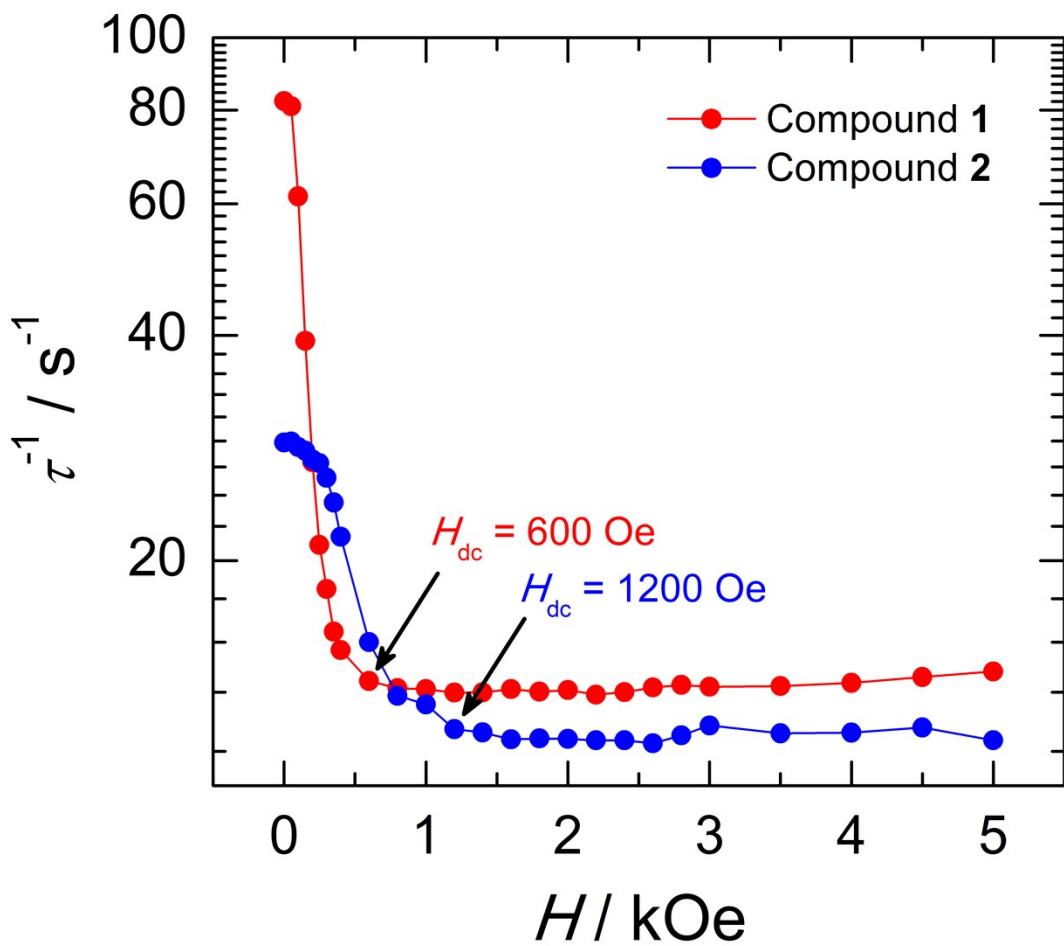


**Figure S19.** Field dependence of the relaxation times ( $\tau$ ) at a fixed temperature of 20 K for compound 1 (red) and compound 2 (blue). The relaxation times were obtained from the generalized Debye model (see, Tables S12-S13). The minimum represents the optimal static field for which the relaxation time is longest and quantum tunneling of the magnetization is reduced. This is the field at which temperature dependent relaxation studies were completed at (*vide infra*).

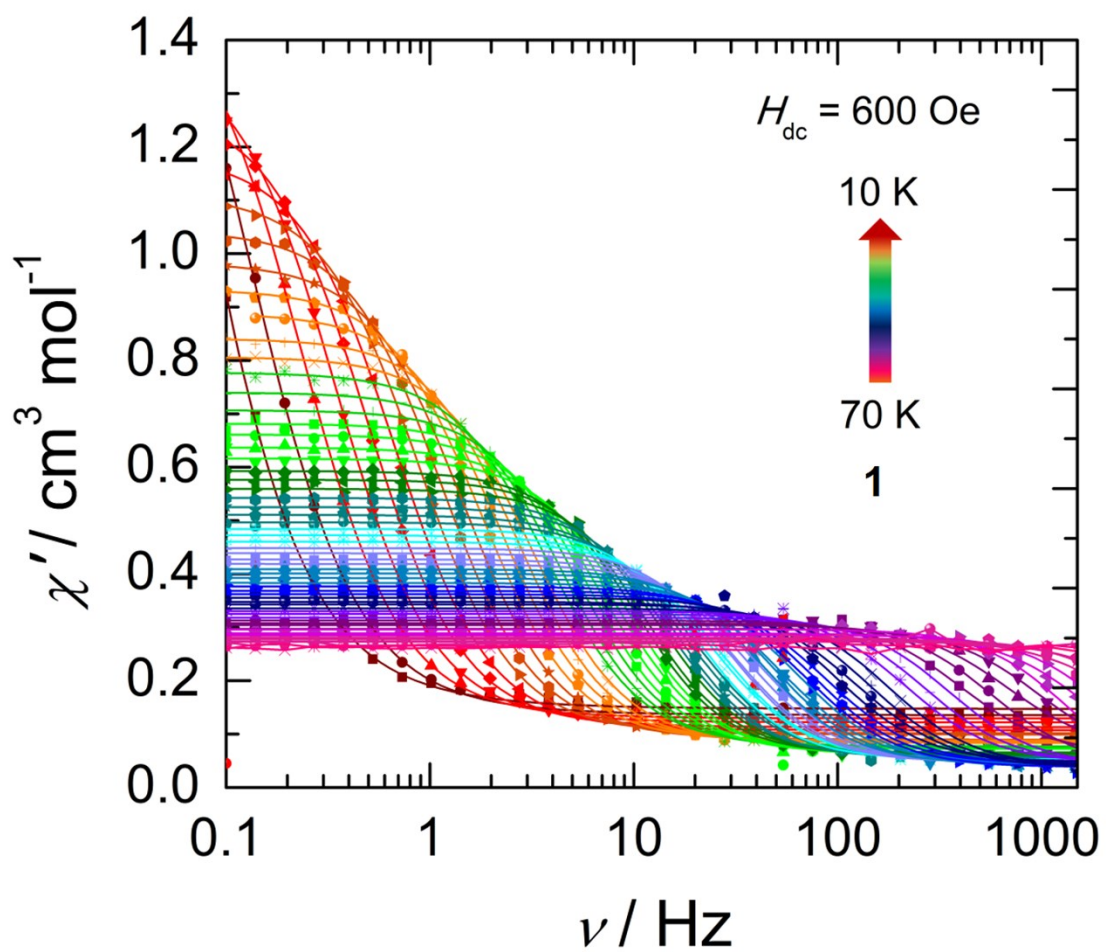


**Figure S20.** Frequency dependence of  $\chi'$  as a function of temperature in the range 10-70 K, under an applied static field of 600 Oe for compound **1**. Solid lines represent best fits to the generalized Debye model. Best fit parameters are summarized in Table S14.

**Table S14.** Best-fit parameters to the generalized Debye model for the frequency dependence of the in-phase magnetic susceptibility ( $\chi'$ ) as a function of temperature for **1** (Figure S20). Data collected under an applied static field ( $H_{dc} = 600$  Oe). Values in red were restrained in order to remain physically reasonable. Where no values are present, no reasonable fit could be obtained.

T (K)	$\tau$ (s)	$\alpha$	$\chi_T$	$\chi_s$	$\chi_T - \chi_s$
10	2.45888	0.09414	2.46657	0.14743	2.31913
11	1.20695	0.07456	1.82091	0.13565	1.68527
12	0.6909	0.04867	1.5251	0.12949	1.39561
13	0.46329	0.03905	1.38155	0.12213	1.25941
14	0.3279	0.0354	1.27565	0.113	1.16265
15	0.24006	0.0297	1.18478	0.10742	1.07735
16	0.18166	0.02799	1.11012	0.10177	1.00835
17	0.14089	0.02049	1.04275	0.09933	0.94342
18	0.11034	0.02605	0.98356	0.08976	0.89381
19	0.08882	0.02401	0.93351	0.08776	0.84575
20	0.0727	0.02185	0.88852	0.08693	0.80158
21	0.05936	0.011	0.84073	0.08642	0.75431
22	0.05017	0.01688	0.80669	0.08357	0.72311
23	0.04248	0.02884	0.7779	0.07719	0.70071
24	0.03612	0.016	0.74006	0.07544	0.66462
25	0.03036	0.00864	0.70664	0.07421	0.63244
26	0.02653	0.00717	0.68146	0.07216	0.60931
27	0.02293	0.01771	0.66146	0.0641	0.59735
28	0.02007	0.01792	0.63707	0.06451	0.57256
29	0.01752	0.01253	0.61647	0.06095	0.55552
30	0.01557	0.00893	0.59292	0.0622	0.53072
31	0.01425	0	0.57647	0.06565	0.51082
32	0.01219	0.01079	0.55965	0.05805	0.5016
33	0.01108	0.00937	0.5426	0.05704	0.48557
34	0.00998	0	0.52525	0.0561	0.46915
35	0.009	0.01921	0.51087	0.05557	0.4553
36	0.00809	0.01311	0.4968	0.05346	0.44334
37	0.00751	8.92E-04	0.4842	0.05266	0.43154
38	0.00656	0.02195	0.47294	0.05	0.42294
39	0.00605	0.00761	0.46048	0.05109	0.40939
40	0.00531	0	0.44827	0.04783	0.40044
41	0.0051	0	0.43878	0.05093	0.38785
42	0.00447	0.00526	0.42743	0.05011	0.37732
43	0.00392	0.01766	0.41884	0.04502	0.37382
44	0.00368	0.00663	0.40914	0.04476	0.36438

45	0.00325	0.00379	0.40094	0.04305	0.35789
46	0.00306	0.01249	0.39243	0.04649	0.34594
47	0.00249	0.01601	0.38328	0.03842	0.34486
48	0.0023	0.02227	0.37671	0.03783	0.33888
49	0.00207	0	0.36815	0.04521	0.32293
50	0.0018	0.02003	0.36236	0.04188	0.32047
51	0.00158	0	0.35547	0.04817	0.30729
52	0.00129	0.03075	0.34808	0.03684	0.31124
53	0.00112	0	0.34298	0.04214	0.30084
54	8.91E-04	0	0.33549	0.03898	0.29651
55	7.32E-04	0	0.33038	0.04727	0.28311
56	5.88E-04	0	0.32479	0.04446	0.28034
57	4.52E-04	0	0.31826	0.0409	0.27736
58	3.95E-04	0	0.3127	0.06347	0.24923
59	2.80E-04	0	0.30763	0.0407	0.26694
60	2.34E-04	0	0.30415	0.07026	0.23389
61	1.64E-04	0	0.29735	0.05204	0.24531
62	1.16E-04	3.48E-22	0.29607	0	0.29607
63	8.70E-05	0.03493	0.28902	0	0.28902
64	7.19E-05	0	0.28557	0	0.28557
65	4.92E-05	0.06707	0.28121	0	0.28121
66	4.42E-05	0	0.27713	0	0.27713
67	5.02E-05	0	0.27309	0.09161	0.18148
68	--	--	--	--	--
69	--	--	--	--	--
70	--	--	--	--	--

**Table S15.** Best-fit parameters to the generalized Debye model for the frequency dependence of the out-of-phase magnetic susceptibility ( $\chi''$ ) as a function of temperature for **1** (Figure 4e). Data collected under an applied static field ( $H_{dc} = 600$  Oe). Values in red were restrained in order to remain physically reasonable.

T (K)	$\tau$ (s)	$\alpha$	$\chi_T$	$\chi_s$	$\chi_T - \chi_s$
10	1.85252	0.05613	2.37541	0.65451	1.7209
11	1.03942	0.03021	2.2171	0.75484	1.46226
12	0.66098	0.02703	1.95211	0.62338	1.32873
13	0.45466	0.02168	1.83185	0.60824	1.22361
14	0.32434	0.01982	1.66708	0.53291	1.13418
15	0.23937	0.01795	1.12482	0.06715	1.05768
16	0.18163	0.02012	1.02341	0.02785	0.99556
17	0.14005	0.01026	0.9293	2.81E-05	0.92928
18	0.11045	0.01762	1.003	0.11891	0.88409
19	0.08894	0.01997	0.83978	6.96E-04	0.83908
20	0.07262	0.01451	0.79772	0.00366	0.79405
21	0.0596	0.02058	0.7598	0.00142	0.75837
22	0.04995	0.01264	0.72226	7.90E-04	0.72147
23	0.04249	0.00512	0.68518	5.99E-04	0.68458
24	0.03574	0.01377	0.71863	0.052	0.66664
25	0.03062	0.01504	0.64029	0.00265	0.63764
26	0.02661	0.00527	0.65217	0.04269	0.60948
27	0.02286	0.01291	0.59349	4.12E-05	0.59345
28	0.02033	0.00646	1.08451	0.51856	0.56595
29	0.01747	0.01605	0.55108	3.33E-04	0.55075
30	0.01589	0	0.52426	2.87E-05	0.52423
31	0.01377	0.01516	0.51866	5.24E-04	0.51813
32	0.01224	0.01508	0.50367	0.00712	0.49655
33	0.01084	0.02019	0.52372	0.03429	0.48943
34	0.01004	0.0053	0.47173	0.00629	0.46544
35	0.00893	0.01146	0.46018	0.00129	0.45889
36	0.00799	0.01716	0.45179	6.42E-04	0.45115
37	0.00747	0.00947	0.43225	0.0023	0.42995
38	0.00667	0.00681	0.44717	0.02718	0.41999
39	0.00605	0.0124	0.46399	0.05468	0.40931
40	0.00544	0.01517	0.40216	2.18E-05	0.40213
41	0.00493	0.01398	0.39357	4.05E-04	0.39316
42	0.00462	0.00618	0.38917	0.01112	0.37805
43	0.00417	0.02636	0.36595	0.00117	0.36477
44	0.00374	0.00956	0.36166	1.07E-04	0.36155

45	0.00336	0.01848	0.3637	0.01299	0.35071
46	0.003	0.00926	0.35397	0.00247	0.3515
47	0.00269	0	0.53927	0.19776	0.34151
48	0.00243	0.00828	0.34163	0.0079	0.33373
49	0.00216	0	0.34904	0.0157	0.33334
50	0.0019	0	0.32858	0.01525	0.31333
51	0.00158	0	0.33572	0.01962	0.3161
52	0.00136	0	0.33599	0.02307	0.31292
53	0.00108	0.01176	0.32682	0.02421	0.30261
54	8.92E-04	0.01326	0.32629	0.02627	0.30002
55	7.14E-04	0	0.32111	0.02893	0.29218
56	5.65E-04	0.00962	0.32095	0.03789	0.28306
57	4.52E-04	0.00272	0.31912	0.03891	0.28021
58	3.61E-04	0	0.30959	0.04262	0.26697
59	2.54E-04	0.05062	0.50328	0.20061	0.30267
60	2.17E-04	0	0.30871	0.0496	0.25911
61	1.22E-04	0.10856	0.34874	0.03194	0.3168
62	1.33E-04	0	0.30451	0.05074	0.25378
63	1.05E-04	0.01746	0.29795	0.04569	0.25226
64	5.37E-05	0.05003	0.33642	0.00689	0.32953
65	5.81E-05	0	0.28928	0.02405	0.26522
66	6.85E-05	0	0.33483	0.17128	0.16355
67	1.64E-05	0	0.55956	0	0.55956
68	4.75E-05	0	0.22713	0.08507	0.14205
69	2.73E-06	0.03062	1.92615	0	1.92615
70	1.36E-05	0	0.32798	0	0.32798

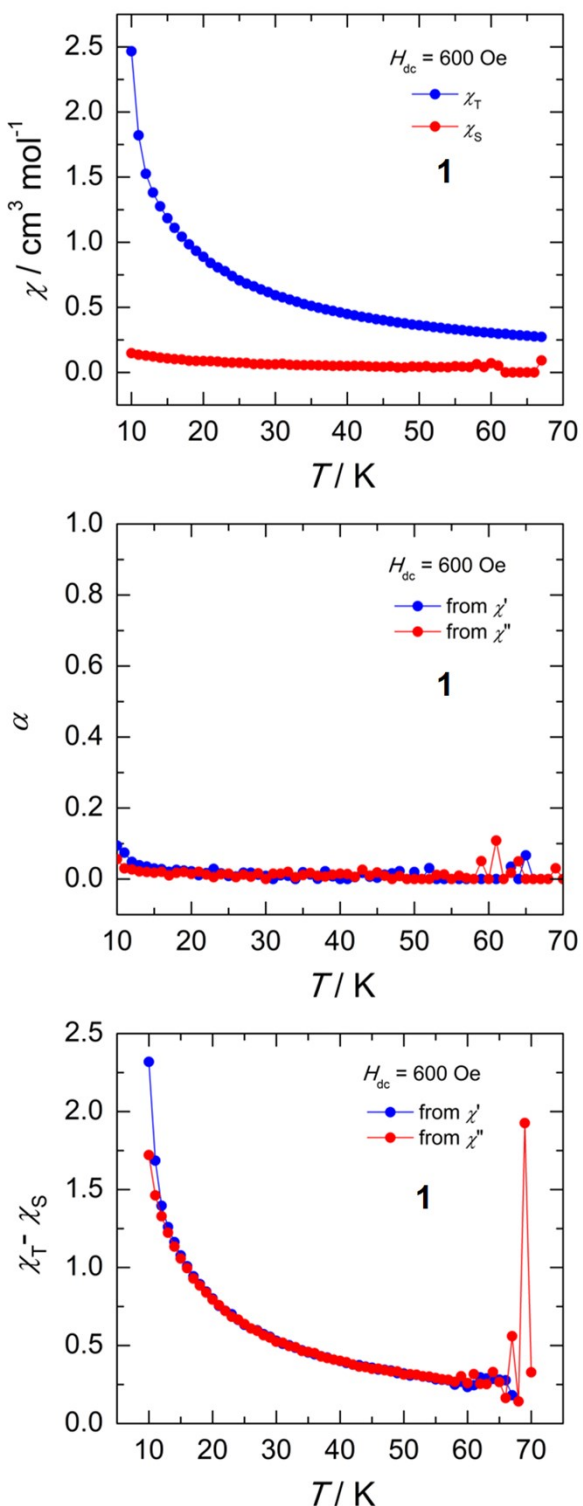


**Figure S21.** Data obtained from the generalized Debye fits of  $\chi'$  and  $\chi''$  frequency dependent ac data collected under an applied static field ( $H_{dc} = 600$  Oe) for compound **1**. Temperature dependence of  $\chi_T$  and  $\chi_S$  (*top*),  $\alpha$  (*middle*), and  $\chi_T - \chi_S$  (*bottom*).

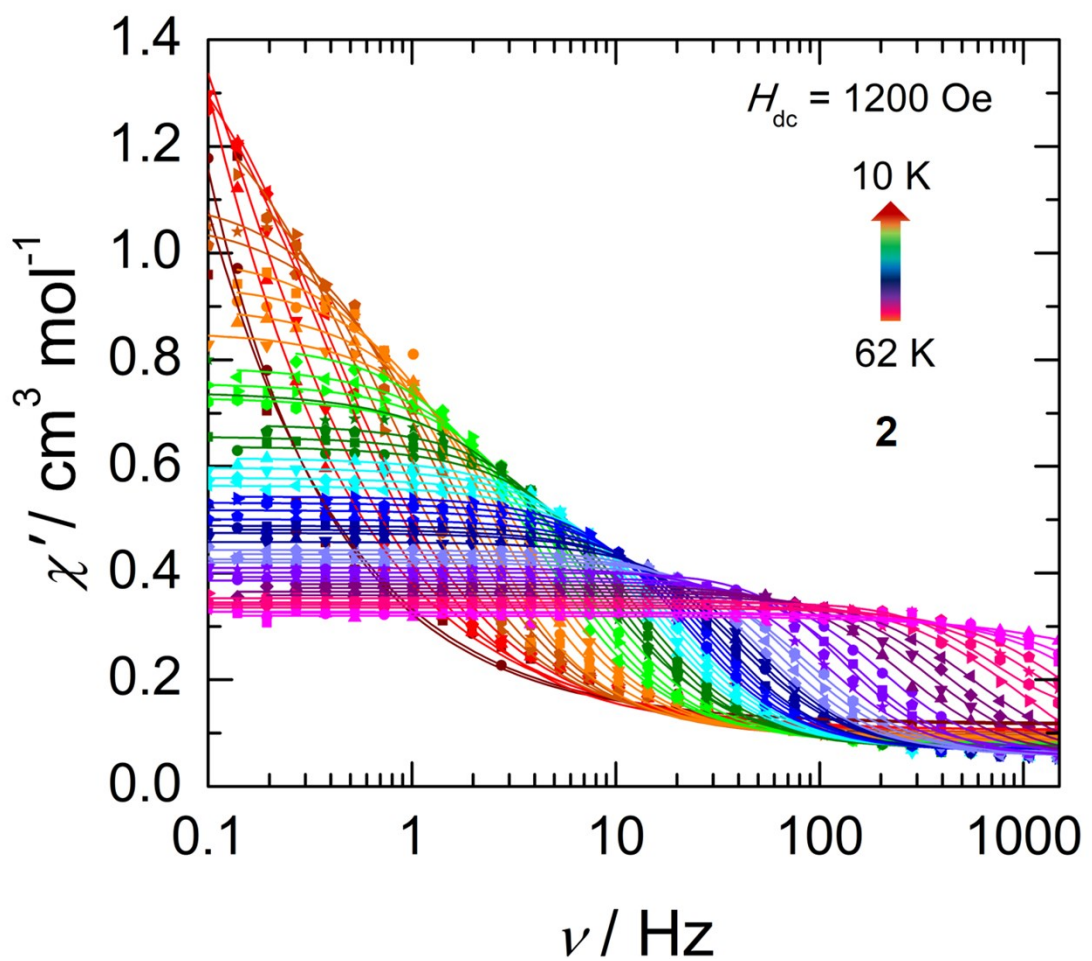


**Figure S22.** Frequency dependence of  $\chi'$  as a function of temperature in the range 10-70 K, under an applied static field of 1200 Oe for compound 2. Solid lines represent best fits to the generalized Debye model. Best fit parameters are summarized in Table S16.

**Table S16.** Best-fit parameters to the generalized Debye model for the frequency dependence of the in-phase magnetic susceptibility ( $\chi'$ ) as a function of temperature for **2** (Figure S22). Data collected under an applied static field ( $H_{dc} = 1200$  Oe). Values in red were restrained in order to remain physically reasonable.

T (K)	$\tau$ (s)	$\alpha$	$\chi_s$	$\chi_r$	$\chi_r - \chi_s$
10	8.06121	0.37065	0.11402	4.60867	4.49465
11	7.5	0.35877	0.1128	4.90794	4.79514
12	5.60904	0.36999	0.10271	4.61388	4.51117
13	1.22553	0.32261	0.10462	2.30764	2.20303
14	0.4363	0.23787	0.10621	1.58187	1.47565
15	0.43096	0.26938	0.0999	1.63359	1.53369
16	0.26546	0.2299	0.09976	1.38874	1.28898
17	0.19599	0.21773	0.09396	1.27369	1.17973
18	0.12417	0.1641	0.09607	1.1131	1.01703
19	0.1054	0.16996	0.08895	1.06902	0.98007
20	0.08614	0.13583	0.09349	0.99825	0.90476
21	0.06643	0.12886	0.09075	0.94573	0.85498
22	0.05526	0.14443	0.08506	0.90292	0.81786
23	0.04563	0.13618	0.08366	0.85445	0.77079
24	0.03959	0.1444	0.08057	0.83476	0.75419
25	0.03268	0.13076	0.07901	0.78803	0.70901
26	0.0276	0.12225	0.0768	0.75713	0.68033
27	0.02365	0.13377	0.07427	0.73019	0.65591
28	0.02274	0.17173	0.07103	0.74074	0.66971
29	0.01797	0.10917	0.07546	0.67952	0.60406
30	0.01532	0.11486	0.06788	0.65675	0.58887
31	0.01369	0.11442	0.0698	0.6381	0.5683
32	0.01194	0.1102	0.06811	0.61637	0.54827
33	0.01066	0.10039	0.06964	0.59767	0.52803
34	0.00938	0.09818	0.07004	0.57902	0.50898
35	0.00833	0.10721	0.06463	0.56456	0.49994
36	0.00744	0.08187	0.06969	0.54383	0.47414
37	0.00675	0.08971	0.0642	0.53205	0.46784
38	0.00599	0.08725	0.06431	0.51832	0.45401
39	0.00537	0.07647	0.06552	0.50086	0.43535
40	0.00488	0.06334	0.06563	0.4888	0.42317
41	0.00423	0.10017	0.06117	0.48199	0.42082
42	0.00387	0.09965	0.05905	0.47554	0.41649
43	0.00333	0.07057	0.06134	0.45836	0.39702
44	0.003	0.05084	0.06374	0.44326	0.37952

45	0.00252	0.06608	0.05632	0.43552	0.37921
46	0.00216	0.0491	0.0622	0.42593	0.36374
47	0.00189	0.08697	0.05428	0.42019	0.36591
48	0.00155	0.06397	0.05649	0.40965	0.35317
49	0.00123	0	0.06934	0.40074	0.33139
50	0.00106	0.04682	0.05337	0.39276	0.33939
51	8.18754E-4	0.06288	0.05534	0.38616	0.33083
52	6.33454E-4	0.0763	0.05191	0.37918	0.32726
53	4.68006E-4	0.09533	0.04563	0.37216	0.32653
54	3.80219E-4	0.08574	0.05	0.36532	0.31532
55	2.89257E-4	0.09073	0.04858	0.35823	0.30965
56	1.67386E-4	0.14271	0	0.35287	0.35287
57	2.33678E-4	2.66423E-21	0.12661	0.34476	0.21815
58	1.23313E-4	0.11368	0.0531	0.34047	0.28737
59	7.96956E-5	0.12643	0	0.3355	0.3355
60	5.34895E-5	0.15798	0	0.32743	0.32743
61	3.87604E-5	0.19357	0	0.32536	0.32536
62	1.64706E-5	0.28729	0	0.32022	0.32022

**Table S17.** Best-fit parameters to the generalized Debye model for the frequency dependence of the out-of-phase magnetic susceptibility ( $\chi''$ ) as a function of temperature for **2** (Figure 4f). Data collected under an applied static field ( $H_{dc} = 1200$  Oe). Values in red were restrained in order to remain physically reasonable.

T (K)	$\tau$ (s)	$\alpha$	$\chi_T$	$\chi_s$	$\chi_T - \chi_s$
10	1.32325	0.21848	0.19669	1.60517	1.40848
11	1.47256	0.18267	0.06105	1.80699	1.74595
12	0.84388	0.14823	0.60968	2.10086	1.49119
13	0.57659	0.18419	0.14333	1.55786	1.41452
14	0.41319	0.19034	0.1418	1.44368	1.30188
15	0.30339	0.16934	0.01003	1.22586	1.21583
16	0.22678	0.1594	0.31107	1.4423	1.13123
17	0.16698	0.1534	0.05155	1.09746	1.04591
18	0.13577	0.07682	0.00307	0.9197	0.91664
19	0.10499	0.13297	0.10424	1.038	0.93376
20	0.08424	0.12354	0.05067	0.92336	0.87268
21	0.06886	0.11668	0.00793	0.83395	0.82602
22	0.05658	0.11961	0.01017	0.79479	0.78462
23	0.04739	0.11478	0.013	0.77252	0.75952
24	0.03869	0.09368	0.00154	0.70877	0.70723
25	0.03299	0.12497	0.16036	0.86294	0.70258
26	0.02811	0.1061	9.49351E-4	0.66917	0.66822
27	0.02325	0.08628	0.0345	0.65781	0.62332
28	0.02083	0.10675	0.02891	0.65005	0.62114
29	0.01825	0.10338	2.7102E-4	0.59909	0.59882
30	0.01567	0.11188	0.00564	0.58992	0.58429
31	0.01383	0.10794	0.00152	0.56672	0.56519
32	0.01222	0.09457	3.39084E-4	0.54071	0.54037
33	0.01073	0.0925	0.00625	0.53052	0.52426
34	0.00961	0.09869	0.00604	0.51506	0.50902
35	0.00852	0.08818	5.18968E-5	0.4932	0.49315
36	0.00749	0.1013	3.95856E-6	0.48611	0.48611
37	0.00661	0.10226	0.00118	0.47584	0.47466
38	0.00605	0.09257	0.00459	0.45989	0.4553
39	0.00545	0.08298	0.00292	0.44149	0.43858
40	0.00481	0.07995	1.71464E-5	0.43078	0.43077
41	0.00438	0.07394	0.00941	0.42547	0.41606
42	0.00386	0.07369	7.93219E-4	0.40892	0.40812
43	0.00331	0.10143	5.59494E-4	0.40897	0.40841
44	0.00297	0.10509	7.99308E-4	0.39731	0.39651

45	0.00259	0.06144	0.00108	0.38534	0.38425
46	0.00221	0.07788	7.04683E-4	0.37796	0.37726
47	0.00186	0.10478	2.99895E-5	0.37083	0.3708
48	0.00157	0.09448	0.00441	0.36695	0.36254
49	0.00129	0.08484	2.2313E-4	0.34877	0.34855
50	0.00101	0.09827	0.01253	0.36416	0.35163
51	8.17089E-4	0.08074	0.00196	0.34078	0.33882
52	6.02722E-4	0.07595	0.00514	0.3364	0.33126
53	4.74307E-4	0.09816	7.33135E-4	0.32743	0.32669
54	3.77771E-4	0.06494	0.00764	0.32762	0.31998
55	2.98053E-4	0.04786	3.12128E-4	0.30699	0.30668
56	2.02111E-4	0.12124	0.00173	0.3237	0.32197
57	1.38946E-4	0.11522	0.0081	0.33613	0.32803
58	1.52499E-4	0.07853	0.0087	0.28295	0.27425
59	9.04618E-5	0.10737	0.00594	0.3015	0.29556
60	2.44128E-5	0.21862	0	0.5527	0.5527
61	3.5616E-6	0.26435	0	1.44673	1.44673
62	1.11277E-4	0	0	0.14214	0.14214

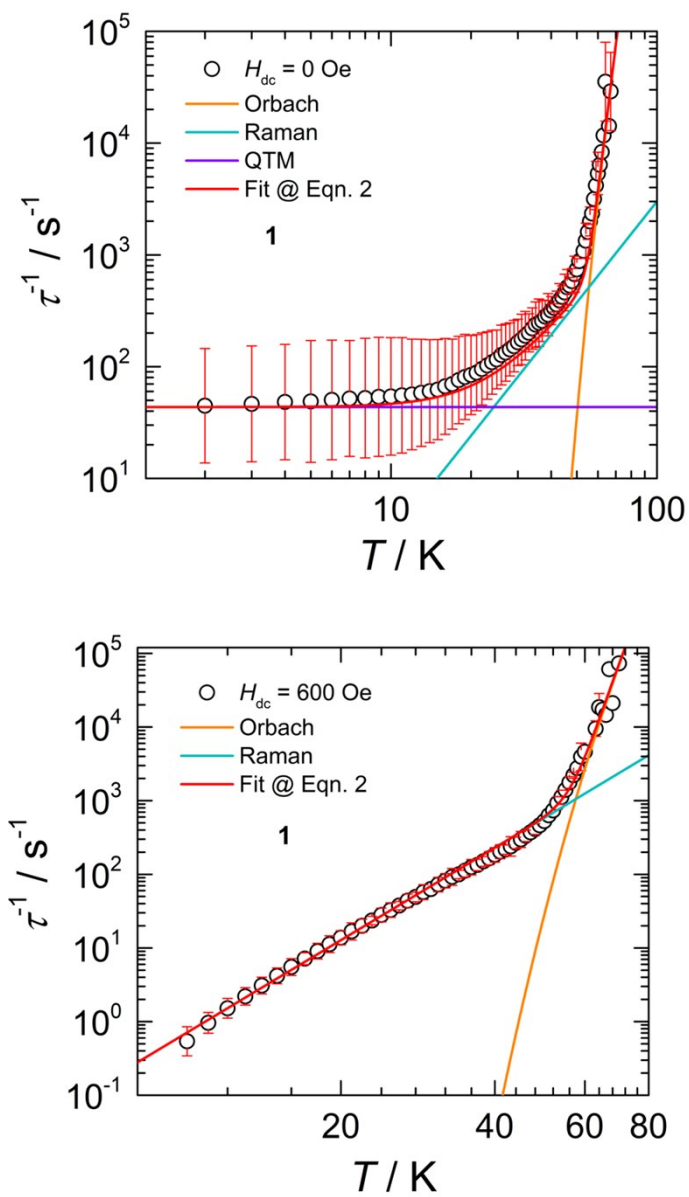


**Figure S23.** Temperature dependence of the relaxation times ( $\tau$ ) for compound **1** collected under zero applied static field ( $H_{\text{dc}} = 0 \text{ Oe}$ ; *top*) and under an applied static field ( $H_{\text{dc}} = 600 \text{ Oe}$ ; *bottom*). The red solid lines represent the best fit to **Eqn. 2 (main text)**. The orange, teal, and purple lines are the individual components of the magnetization relaxation for Orbach, Raman, and quantum tunneling processes, respectively. Best fit parameters are summarized in Table S18. The error bars on the relaxation time have been calculated from the  $\alpha$ -parameters of the generalized Debye fit with the log-normal distribution.

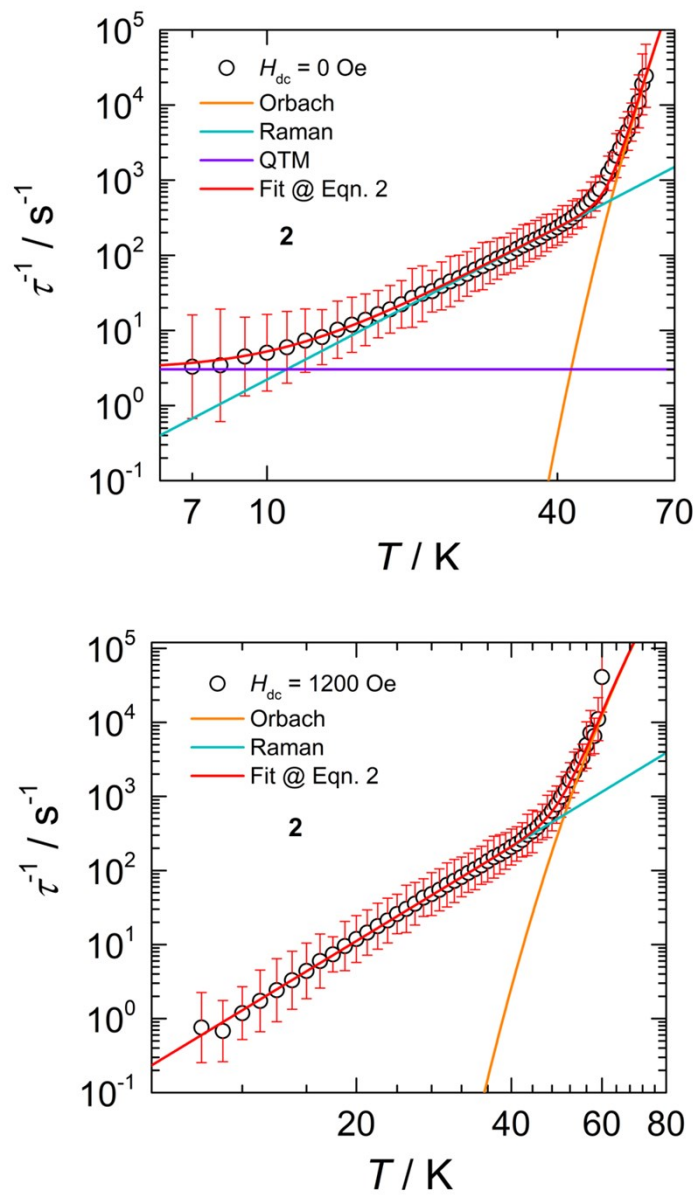


**Figure S24.** Temperature dependence of the relaxation times ( $\tau$ ) for compound **2** collected under zero applied static field ( $H_{dc} = 0$  Oe; *top*) and under an applied static field ( $H_{dc} = 1200$  Oe; *bottom*). The red solid lines represent the best fit to **Eqn. 2 (main text)**. The orange, teal, and purple lines are the individual components of the magnetization relaxation for Orbach, Raman, and quantum tunneling processes, respectively. Best fit parameters are summarized in Table S18. The error bars on the relaxation time have been calculated from the  $\alpha$ -parameters of the generalized Debye fit with the log-normal distribution.

**Table S18.** Magnetic relaxation parameters obtained from the fit of the temperature dependent relaxation times (Figures S23-S24) for compound **1** and **2**. Best fits were obtained with quantum tunneling of the magnetization, Orbach, and Raman contributions (**Eqn. 2, main text**).

		Compound 1		Compound 2	
Parameters		$H_{dc} = 0$ Oe	$H_{dc} = 600$ Oe	$H_{dc} = 0$ Oe	$H_{dc} = 1200$ Oe
QTM	$\tau_{QTM}$	0.023 s	-	0.33 s	-
Orbach	$\tau_0$	$7.01 \times 10^{-14}$ s	$4.81 \times 10^{-14}$ s	$3.37 \times 10^{-14}$ s	$3.58 \times 10^{-12}$ s
	$U_{eff}$	1334 K / 927 cm <sup>-1</sup>	1366 K / 949 cm <sup>-1</sup>	1278 K / 888 cm <sup>-1</sup>	1016 K / 705 cm <sup>-1</sup>
Raman	$C$	$3.01 \times 10^{-3}$ s <sup>-1</sup> K <sup>-n</sup>	$4.80 \times 10^{-5}$ s <sup>-1</sup> K <sup>-n</sup>	$9.89 \times 10^{-4}$ s <sup>-1</sup> K <sup>-n</sup>	$3.61 \times 10^{-5}$ s <sup>-1</sup> K <sup>-n</sup>
	$n$	3.0	4.17	3.35	4.22

## References

- [1] K. Izod, S. T. Liddle, W. Clegg, *Inorg. Chem.* **2004**, *43*, 214-218.
- [2] S. Fortier, J. R. Aguilar-Calderón, B. Vlaisavljevich, A. J. Metta-Magaña, A. G. Goos, C. E. Botez, *Organometallics* **2017**, *36*, 4591-4599.
- [3] SMART Apex II, Version 2.1; Bruker AXS Inc.: Madison, WI
- [4] SAINT Software User's Guide, Version 7.34a; Bruker AXS Inc.: Madison, WI
- [5] Blessing, R. *Acta Crystallogr. A* **1995**, A51
- [6] Sheldrick, G. M. SHELXTL, 6.12; Bruker Analytical X-Ray Systems, Inc.: Madison, WI
- [7] Dolomanov, O. V.; Bourhis, L. J.; Gildea, R. J.; Howard, J. A. K.; Puschmann, H. *J. Appl. Cryst.* **2009**, *42*, 339
- [8] F. Aquilante, J. Autschbach, R. K. Carlson, L. F. Chibotaru, M. G. Delcey, L. De Vico, I. F. Galvan, N. Ferre, L. M. Frutos, L. Gagliardi, M. Garavelli, A. Giussani, C. E. Hoyer, G. Li Manni, H. Lischka, D. Ma, P. A. Malmqvist, T. Mueller, A. Nenov, M. Olivucci, T. B. Pedersen, D. Peng, F. Plasser, B. Pritchard, M. Reiher, I. Rivalta, I. Schapiro, J. Segarra-Marti, M. Stenrup, D. G. Truhlar, L. Ungur, A. Valentini, S. Vancoillie, V. Veryazov, V. P. Vysotskiy, O. Weingart, F. Zapata, R. Lindh, *J. Comput. Chem.* **2016**, *37*, 506-541.
- [9] a) B. O. Roos, R. Lindh, P.-A. Malmqvist, V. Veryazov, P.-O. Widmark, A. C. Borin, *J. Phys. Chem. A* **2008**, *112*, 11431-11435; b) B. O. Roos, R. Lindh, P. A. Malmqvist, V.

- Veryazov, P. O. Widmark, *J. Phys. Chem. A* **2004**, *108*, 2851-2858; c) B. O. Roos, V. Veryazov, P. O. Widmark, *Theor. Chem. Acc.* **2004**, *111*, 345-351.
- [10] a) F. Aquilante, R. Lindh, T. B. Pedersen, *J. Chem. Phys.* **2007**, *127*; b) F. Aquilante, T. B. Pedersen, R. Lindh, B. O. Roos, A. S. De Meras, H. Koch, *J. Chem. Phys.* **2008**, *129*.
- [11] A. Wolf, M. Reiher, *Journal of Chemical Physics* **2006**, *124*.
- [12] B. O. Roos, *The complete active space self-consistent field method and its applications in electronic structure calculations*, John Wiley & Sons, Inc., **2007**.
- [13] B. A. Hess, C. M. Marian, U. Wahlgren, O. Gropen, *Chem. Phys. Lett.* **1996**, *251*, 365-371.
- [14] L. F. Chibotaru, L. Ungur, *J. Chem. Phys.* **2012**, *137*.
- [15] L. Ungur, L. F. Chibotaru, *Chem. Eur. J.* **2016**.